# Microbial community dynamics during a harmful *Chrysochromulina leadbeateri* bloom

Nerea J. Aalto[1,2], Hannah Schweitzer[1,2], Erlend Grann-Meyer[1], Stina Krsmanovic[1], Jon Brage Svenning[1], Lars Dalheim[1], Sebastian Petters[1], Richard Ingebrigtsen[1], Chris J. Hulatt[3], Hans C. Bernstein[1,2]*

**Affiliations:**

*1. Norwegian College of Fisheries Sciences, UiT - The Arctic University of Norway, Tromsø, Norway*

*2. The Arctic Centre for Sustainable Energy, UiT - The Arctic University of Norway, Tromsø, Norway*

*3. Faculty of Biosciences and Aquaculture, Nord University, Bodø, Norway*

***Correspondence**: Hans C. Bernstein, UiT-The Arctic University of Norway, BFE-fak., Postboks 6050 Langnes, 9037 Tromsø, NORWAY*; Phone: +47 776 46 114; Email:* Hans.C.Bernstein@uit.no

***Running Title:*** Ecology of the Norwegian harmful algae bloom of 2019

***Keywords:*** Marine Microbiome, Harmful Algae, Aquaculture, Norway, Time Series Analysis

**ABSTRACT**

In late spring 2019 a harmful algae bloom occurred across multiple, interconnected fjords and bays in northern Norway. This was a major event causing severe fish mortality at several salmon aquaculture facilities in the region. The reported focal taxon and suspected agent of fish mortality was a *Chrysochromulina leadbeateri*-like prymnesiophyte that was morphologically identical to the UiO-035 isolate collected from a similar bloom from the same region in 1991. This study reports on succession dynamics of the marine microbiome via detectable changes in abundance of 18S and 16S rRNA gene amplicon sequence variants and closely related taxa of the focal strain *C. leadbeateri* UiO-035. This taxon co-bloomed with a diverse group of microeukaryotes and prokaryotes and their temporal succession dynamics revealed high variability with strong shifts in abundance during the event. These blooming patterns were poorly connected to environmental conditions suggesting that other factors such as biological interactions may be at least as important in shaping the dynamics of this type of harmful algae bloom. A deeper understanding of microbiome succession patterns during these rare but destructive bloom events will help guide future efforts to generate predictive models and anticipate deviations from the natural bloom cycles of the northern Norwegian fjord systems that are home to large scale aquaculture activities.

## INTRODUCTION

Harmful algal blooms (HABs) are common in warm and temperate waters, but also occur in northern cold water ecosystems (Hallegraeff et al., 2021; Karlson et al., 2021). These blooms pose a serious risk for aquaculture activities, because farmed fish cannot escape from developing adverse conditions caused by marine microalgae. Previously, the most infamous northern Norwegian bloom occurred in 1991 in Ofotfjord causing high mortality in affected fish farms (Rey, 1991). Smaller HAB incidents have occurred since then, although they have gained little mainstream attention (Grann-Meyer, 2020). The salmon aquaculture industry has expanded tremendously over the past decades to a landing value of salmon that reached 7 billion USD in 2019 (Statistics Norway, 2020). While this has caused concern, it has not spurred investments in long-term monitoring of algal bloom dynamics or occurrence of potentially harmful algae species in areas that support salmon aquaculture. Therefore, most stakeholders were taken by surprise when a deadly HAB of *Chrysochromulina leadbeateri* (prymnesiophyte) reoccurred and caused massive fish mortalities in the Troms and Nordland regions of costal northern Norway from mid-May to the beginning of June 2019 (Karlsen et al., 2019). The fish loss was ca. 14 500 tonnes, which is the highest amount among fish kill related HABs in Scandinavia since 1988 (Karlsen et al., 2019; Karlson et al., 2021). Thus, knowledge that can eventually inform causation is very limited, especially in the context of seasonal microbial blooming dynamics, detailed taxonomy of co-blooming species, and the environmental conditions during the 2019 incident.

Marine HABs are often associated with altered ratios of inorganic nitrogen-to-phosphate (N:P), coupled with a long period of high irradiance, calm weather, and strong surface water stratification (Nielsen et al., 1990; Anderson et al., 2002; Uronen et al., 2005). However, the role of N:P ratio in determining the magnitude, frequency, and duration of HABs has been questioned (Davidson et al., 2012) as more evidence is showing that abiotic conditions

are not the only influencing factors of microalgal bloom dynamics. The importance of intra- and interspecific interactions between members of the marine microbiome has become well recognized as a major factor in structuring the temporal and spatial relationships of phytoplankton communities (e.g., Needham and Fuhrman, 2016; Martin-Platero et al., 2018; Aalto et al., 2022). These interactions can be complex and subject to rapid change within a marine microbial ecosystem. Although they are difficult to disentangle, they have the potential to stimulate, enhance, and/or perpetuate the bloom of specific taxa associated with HABs. Therefore, it is important (yet uncommon today) to observe and catalogue the blooming patterns of whole microbiomes while studying the ecology of focal taxa involved with HAB events.

High-resolution (densely sampled) time series analysis combined with high-resolution taxonomic screening such as 16S and 18S ribosomal RNA gene amplicon sequencing variants or operational taxonomic unit-based diversity is an important method for evaluating microbial succession dynamics and ecological factors that drive blooms at different time scales (Fuhrman et al., 2015; Martin-Platero et al., 2018). However, knowledge about the nature of taxon-specific and non-specific interactions with HAB species is poor, because identification of these "hidden" patterns of interactions in dynamic and species rich communities is challenging. Therefore, an increasing number of modern analytical tools has been developed to apply with time series analysis. For example, WaveClust (Martin-Platero et al., 2018) and k-medoid (Kaufman and Rousseeuw, 2009; Coenen et al., 2020) are applicable and promising approaches to infer both temporal dynamics and networks of microbial interactions.

The specific mechanisms of how HABs cause fish mortality are often unknown and difficult to identify, as was the case for the 1991 and 2019 *C. leadbeateri* HABs in northern Norway (Meldahl et al., 1994; Edvardsen and Paasche, 1998). In fact, the toxicity of many well-known toxic prymnesiophytes – such as *Chrysochromulina* spp. – are not known to be dependent on cell density, which makes detection difficult (Edvardsen and Paasche, 1998). The

100 role that bacteria may play in bloom toxicity is also not clear (Uribe and Espejo, 2003). For
101 example, it has been suggested that toxin biosynthesis in dinoflagellate cells is indirectly
102 mediated by associated bacterial consortia (Green et al., 2004). Heterotrophic bacteria have
103 been shown to increase activity and biomass concentrations during a HAB due to the release of
104 dissolved organic matter from lysed microalgal competitors (Uronen et al., 2007). In order to
105 increase their supply of nutrients, many bacteria also exhibit target-specific or non-specific
106 algicidal activity that inhibit the growth or lyse microalgae; potentially even terminating HABs
107 (Doucette et al., 1999; Meyer et al., 2017). Several known marine algicide bacteria are found
108 in bloom-associated groups such as *Flavobacteria* (*Bacteroidetes*), *Alphaproteobacteria* and
109 *Gammaproteobacteria* (Mayali and Azam, 2004). However, not all bacteria-algae interactions
110 are negative. Several mutualistic and growth enhancing relationships have also been identified,
111 which include metabolite exchange of vitamins and growth hormones from bacteria that trade
112 with microalgae for amino acids and dissolved organic carbon (Cirri and Pohnert, 2019).

113 The spring-summer phytoplankton seasonal succession along the coast of northern
114 Norway has been extensively studied in the past 40 years with specific focus on spring bloom
115 dynamics. The majority of data collected to-date has used only morphology-based identification
116 of microalgal taxa, which has limited the extent to which the full diversity of these communities
117 has been described (Eilertsen et al., 1981; Reigstad and Wassmann, 1996; Degerlund and
118 Eilertsen, 2010; Aalto et al., 2021). From previous studies, we know that the onset of the "spring
119 bloom" occurs in late March/early April, and it is driven by increased irradiance as the region
120 undergoes a shift from polar night to spring, which results in elevated winter nutrient
121 concentrations and a well-mixed water column (Eilertsen and Taasen, 1984; Eilertsen and
122 Frantzen, 2007; Aalto et al., 2021). This leads to a rapid and intense increase of many chain
123 forming centric diatoms that co-bloom with *Phaeocystis pouchetii* (haptophyte), who often
124 outlasts the diatoms and persists throughout the summer (Degerlund and Eilertsen, 2010). The

125 spatial and interannual variation of the late bloom (May-June) phytoplankton community can
126 comprise a diverse mix of low-nutrient-tolerant, heterotrophic, and mixotrophic species
127 belonging to dinoflagellates, cryptophytes, ciliates, and other small flagellates (Eilertsen et al.,
128 1981; Aalto et al., 2021). HAB incidents in northern Norway tend to occur after the primary
129 spring diatom bloom, although historical sampling of these events is sparse and the onset and
130 development of HAB conditions is essentially unknown for the region.

131 Our aim was to contribute to the knowledge of the ecology and microbial succession
132 dynamics associated with the *C. leadbeateri* HAB, which has now proven to be a reoccurring
133 and devastating event in northern Norway. This was accomplished by asking three targeted
134 research questions: i) how did the marine microbiome composition change during the 2019
135 HAB event in relative relation to the focal taxon?; (ii) what were the major blooming (temporal)
136 patterns among prokaryotes and microeukaryotes and which taxa co-bloomed with the focal
137 taxon?; and iii) which environmental factors were associated with the observable differences in
138 the marine microbiome composition? This study represents the first molecular ecology-based
139 investigation of a *C. leadbeateri* HAB and presents new insights into a seasonal marine
140 microbial ecosystem that can have a major impact on the social-economic welfare of Norway
141 through its relation to the aquaculture industry.

142

143 **MATERIALS AND METHODS**

144 **Study areas and sample collection.** Time series sampling was performed between May 27$^{th}$
145 (sample day 0) and June 21$^{st}$ (sample day 25) in 2019, at two primary stations (Supplementary
146 Table S1). The first station was named Grøtsund sampling station (**GSSS**, 69.80 N, 19.36 E).
147 The second station, named as Finnfjord sampling station (**FSS**, 69.19 N, 18.03 E), is located 60
148 km south of GSSS, within the same interconnected fjord-sound system (Figure 1a). Samples
149 were collected from each station twice a week, except station FSS was sampled once in the

150 second sampling week (starting the week of May 27th, 2019), from fixed sampling depth of 10
151 m using a 1.7 L Niskin bottle to get approximately 8.5 L of seawater. The collected seawater
152 was prefiltered for large biomass with a 150 µm plankton mesh, and transported to shore in a
153 15 L Nalgene plastic carboy. All sampling equipment was rinsed with 2% bleach prior and
154 between each sampling effort followed by a rinsing with MilliQ water and a minimum of two
155 volumes of station sampling water prior to collection. Temperature and salinity profiles down
156 to 15–50 m were recorded with a hand-held AML oceanographic X2 electron conductivity-
157 temperature-depth (CTD) instrument (AML Oceanographic, Canada). Seawater particles – i.e.
158 microbial biomass – was collected by vacuum filtration onto 0.22 µm polycarbonate filters (GE
159 Healthcare Whatman 47 mm Nucleopore Polycarbonate Track Etched Membranes; GE
160 Healthcare 111106). All filtering was done inside a sterile laminar flow hood, and the total
161 filtered volume per sample varied from 500 – 750 mL depending on turbidity. Filters were
162 immediately flash frozen and stored at -80 °C. All filtering equipment was disinfected with 2%
163 bleach prior and between sampling efforts and thereafter rinsed with MilliQ water. Water
164 samples for macronutrients: silicate ($Si(OH)_4$), phosphate ($PO_4^{3-}$), and nitrate + nitrite ($NO_3^-$ +
165 $NO_2^-$), were filtered through 47 mm GF/F glass microfiber filters (Whatman) into Falcon tubes
166 using disposable syringes and thereafter stored at -20 °C.

167 In addition to the time series samples from FSS and GSSS, filtered microbial biomass
168 was collected from eight separate locations as single time points between May 27th and June
169 21st (Figure 1a and Supplementary Table S1). The data of these samples is not included within
170 time series analyses but used to compare the 2019 HAB affected area via spatial variation in
171 the relative abundance of the focal taxon and associated microbial communities. The DNA
172 extraction and downstream analysis of all samples were performed at the UiT – The Arctic
173 University of Norway as described below.

174

175 **Environmental factors**. The vertical surface water properties from the time series sampling
176 stations (FSS and GSSS) were inspected using CTD-profile data (Supplementary Figure S1 and
177 S2). The difference in surface water stratification between sampling stations was determined
178 by calculating the mixed layer depth (MLD) from each CTD-profile data using potential
179 density. The depth of 1 m was used as a reference depth as the deployed handheld CTD-sensor
180 enables measurements near surface. A density threshold of 0.1 kg $m^{-3}$ was used to define MLD
181 – i.e. the depth below 1 m where density first exceed the defined threshold (Peralta-Ferriz and
182 Woodgate, 2015). Temperature and salinity values from the depth of 10 m (corresponding the
183 depth of collected biomass) as well as MLD values were further used in statistical analyses. As
184 the CTD-casts between sampling days 11 and 17 were unsuccessful, temperature, salinity, and
185 MLD values for these days were interpolated using the R function 'na.approx' from the R
186 package 'zoo' to fill the missing values. Nutrient concentrations were analyzed 20 months later
187 at the UiT – The Arctic University of Norway with a Quaatro39 autoanalyser (Seal Analytical,
188 UK). $PO_4^{3-}$ concentrations below the detection limit of 0.04 µmol $L^{-1}$ were replaced with a small
189 value (0.001) to enable the estimation of this variable in statistical analysis.
190
191 **Unialgal control cultures.** Controls were performed with the *Chrysochromulina leadbeateri*
192 UiO-035 (Edvardsen et al., 2011) culture obtained from the Norwegian Culture Collection of
193 Algae (NORCCA) repository and cultivated at 6 °C on f/2 medium (Guillard, 1975), fortified
194 with 20 nM of selenium. The cultured *C. leadbeateri* was isolated from a toxic bloom of 1991
195 in Vestfjorden, northern Norway (Eikrem and Throndsen, 1998). Taxonomic identification of
196 the cultured isolate has been mainly based on scale morphology in comparison to holotype
197 (Estep, 1984) and other previous reports on *C. leadbeateri*-like cells both from northern and
198 southern hemisphere (Eikrem and Throndsen, 1998). Several *Chrysochromulina* species are
199 characterized by species-specific bilayer scales which have been considered a morphotype-

200 specific character (Eikrem and Throndsen, 1998). Cells were collected and processed
201 identically to the environmental samples described below. The 18S amplicon analysis assigned
202 four abundant ASVs comprising these control cultures (>1000 ASV counts in all replicates)
203 (Supplementary Figure S3). All four of these ASVs had identical taxonomic assignments within
204 the SILVA v138.1 database: Family = Prymnesiales, Genus = OLI16029, Species = Unknown.
205 Of these four ASVs, ASV *24a92740c5af4cd5a5ac0db70830fbc0* (hereafter referred to as the
206 "focal ASV") comprised 88 % of the OLI16029 unialgal control (Supplementary Figure S4).
207
208 **Amplicon sequencing**. Genomic DNA was extracted and downstream amplicon sequences
209 were obtained using the same protocol as described in Aalto et al. (2022). All the samples were
210 processed together in accordance with the Earth Microbiome Project protocols (Gilbert et al.,
211 2010) with modifications according to Amaral-Zettler et al. (2009). This included
212 recommended primers and barcodes for the V4 hypervariable region of the 16S SSU rRNA
213 gene using the V4 forward (515F) and V4 reverse (806R) primers, and the V9 hypervariable
214 region of the 18S SSU rRNA was targeted with the V9 forward (1391F) and V9 reverse (EukBr)
215 primers. Biological replicates, four or five, were sequenced on an Illumina MiSeq instrument
216 (Illumina, San Diego, CA) according to (Caporaso et al., 2010) at Argonne National Laboratory
217 (Lemont, IL, USA). The realized length of forward and reverse reads was 151 bp.
218
219 **Amplicon analysis.** The amplicon analyses were performed through the QIIME2 environment
220 and using QIIME2 plugins as previously described (Aalto et al. 2022). Briefly, Illumina reads
221 and the corresponding barcode files were imported and demultiplexed using the Earth
222 Microbiome Project paired end flag. All reads were filtered, de-replicated, and chimera checked
223 using all default parameters in the DADA2 v2021.2.0 (Callahan et al., 2016). Reads were
224 merged and amplicon sequence variants (ASVs) were determined using DADA2 v2021.2.0.

225 The DADA2 statistic on sequence reads is provided in Supplementary Data S1 (osf.io). A 16S
226 and 18S rRNA gene classifier from the SILVA v138.1 database was trained using RESCRIPt
227 (Quast et al., 2012; Robeson et al., 2020). The ASVs were classified with the self-trained
228 classifier database. (Yilmaz et al., 2014). It is noted that the major challenge in 16S and 18S
229 based taxonomy is its dependency on taxonomic resolution limitations of the database. We
230 chose to use all classifications given from the SILVA v138 database because it is a standardized
231 approach. Manual curation of taxonomic classification was beyond the scope of this study.
232
233 **Statistics, clustering and correlation.** All ASVs not assigned to the expected kingdom
234 (*Archaea*, *Bacteria* and *Chloroplast*) were removed along with all mitochondria assignments
235 from 16S data set. ASVs assigned to *Archaea*, *Bacteria*, *Vertebrata* and *Arthropoda* and phyla
236 *Cnidaria*, *Echninodermata*, *Annelida*, *Nematozoa*, *Nemertea*, *Porifera*, *Mollusca*, *Ctenophore*
237 and *Tunicata* or phyla belonging to macroalgae and land plants or land fungi such as *Bangiales*,
238 *Floridephycidae*, *Ochrophyta*, *Phragmoplastophyta*, *Ascomycota*, *Basidiomycota* and
239 *Myxogastria* were removed from the 18S data set. Additional information on number of ASVs
240 and sequencing depths before and after removal of unwanted taxa is provided in Supplementary
241 Table S2. The total number of classified ASVs in FSS for 18S and 16S data set was 900 and
242 1309, respectively, and in GSSS 2196 and 1865, respectively. As an exception regarding
243 correction of taxonomic annotations, classified 16S order *Enterobacterales* was manually
244 changed to closely related order *Alteromondales* as the main genera of this order were
245 *Pseudoalteromonas*, *Colwellia* and *Glaciecola* that are known to be members of
246 *Alteromonadales* (Parte et al., 2020).
247 Downstream analysis was completed in R (R Core Team, 2021), using the 'microeco'
248 (Liu et al., 2021) and 'vegan' packages (Oksanen et al., 2013). This study also made use of the
249 K-medoids clustering method adapted from a previously described approach applied to time

250 series microbiome data to examine distinct temporal trends in blooming patterns within
251 communities (Coenen et al., 2020). Briefly, ASV counts from each sample type – i.e., sampling
252 station (FSS or GSSS) and PCR amplification primer type (16S or 18S) – were preprocessed
253 via z-score and variance stabilizing transformations using the 'DESeq2' package in R (Love et
254 al., 2014). Pairwise distance matrices were calculated by the Euclidean distance prior to
255 partitioning each sample-specific ASV into K clusters according to similarity criterion over the
256 time series. The quality of each cluster per each sample type was assessed via the Calinski-
257 Harabasz index (Supplementary Figure S5) (Lord et al., 2017). Pearson's correlation was used
258 to examine the relationship between each temporal dynamic, represented by medoid taxon
259 (cluster centroids), and environmental measurements but also, to obtain the positively and
260 negatively co-blooming microalgae and bacterial taxa with focal ASV.

261 The difference in microbial communities, i.e. beta-diversity, between sampling stations
262 was measured using unweighted UniFrac distance metric which accounts occurrence -
263 presence/absence of ASV - and phylogenetic diversity (Lozupone et al., 2011). The beta-
264 diversity and relationship between community compositions and environmental factors
265 (temperature, salinity, MLD, $Si(OH)_4$, $PO_4^{3-}$, $NO_3^-$ + $NO_2^-$, and relative abundance of focal
266 taxon (OLI16029)) was visualized and conducted via distance based redundancy analysis
267 (dbRDA). The permutational multivariate analysis of variance (PERMANOVA) was
268 performed to test the (dis)similarity in prokaryotic and microeukaryotic community
269 compositions between stations (pairwise) and within stations (Anderson, 2001). The Tukey test
270 was performed on inorganic nutrients to determine if the mean concentration values were
271 statistically different between stations (Abdi and Williams, 2010).

272

273 **Data repository and reproducible analyses.** All sequencing and environmental data is
274 available on the Open Science Framework (osf.io), along with all R Markdown scripts used for

analyses and graphing (osf.io/4wjhp/). All Supplementary Data S1–S11, referred to in this study, is available and found on osf.io/4wjhp/.

## RESULTS

**Geographical distribution of focal taxon in relation to fish mortality.** The focal taxon was assessed as those ASVs assigned to OLI16029, representing the *Chrysochromulina leadbeateri* UiO-035 unialgal strain within the class *Prymnesiophyceae*. This taxon was detected during the 2019 harmful *C. leadbeateri* bloom in varying relative abundance across the northern Norwegian coast and fjords (Figure 1). It´s abundance varied between 0.4 % and 51.8 % of the microeukaryotic community assessed via 18S amplicon sequencing through the HAB affected region. The highest relative abundances of the focal taxon – recorded in our molecular sampling campaign – were obtained in the northern portion of the HAB affected region that included Middle-Balsfjord, South-Tromsø, GSSS, and Tussøy stations (Figure 1a). The microbial community composition was relatively similar between Middle-Balsfjord, South-Tromsø, and GSSS stations with increased relative abundance of 18S ASVs and 16S ASVs indicative of dinoflagellates (class *Dinophyceae*) and order *Flavobacteriales*, respectively, towards station GSSS (Figure 1b-c). The relative abundance of ASVs belonging to the focal taxon were low in Ballangen (Ofotfjord) where the HAB was first reported to originate with high fish mortality in mid-May (Karlsen et al., 2019). The community structure from Ballangen was also distinct, compared to other samples, as it was dominated by 18S ASVs indicative of centric diatoms notably from the genus *Skeletonema* (class *Mediophyceae*) and 16S ASVs classified within the genera *Pseudoalteromonas* and *Colwellia* (order *Alteromonadales*) (Figure 1b-c and Supplementary Data S2 and S3 (osf.io)). The relative abundance of the focal taxon was higher in samples collected from Sagfjord stations (Anevik, Dyping, Veggfjell, and Middle-Sagfjord), south from Ofotfjord, than in the Ballangen and FSS stations (Figure 1a). The microeukaryotic

community in the Sagfjord location was especially diverse, comprising multiple distinct groups of dinoflagellates and centric diatoms being the most abundant. In contrast to the other sampling locations, the 16S prokaryotic ASVs among the Sagfjord stations were predominantly comprised by the order *Pseudomonadales* (Figure 1b-c).

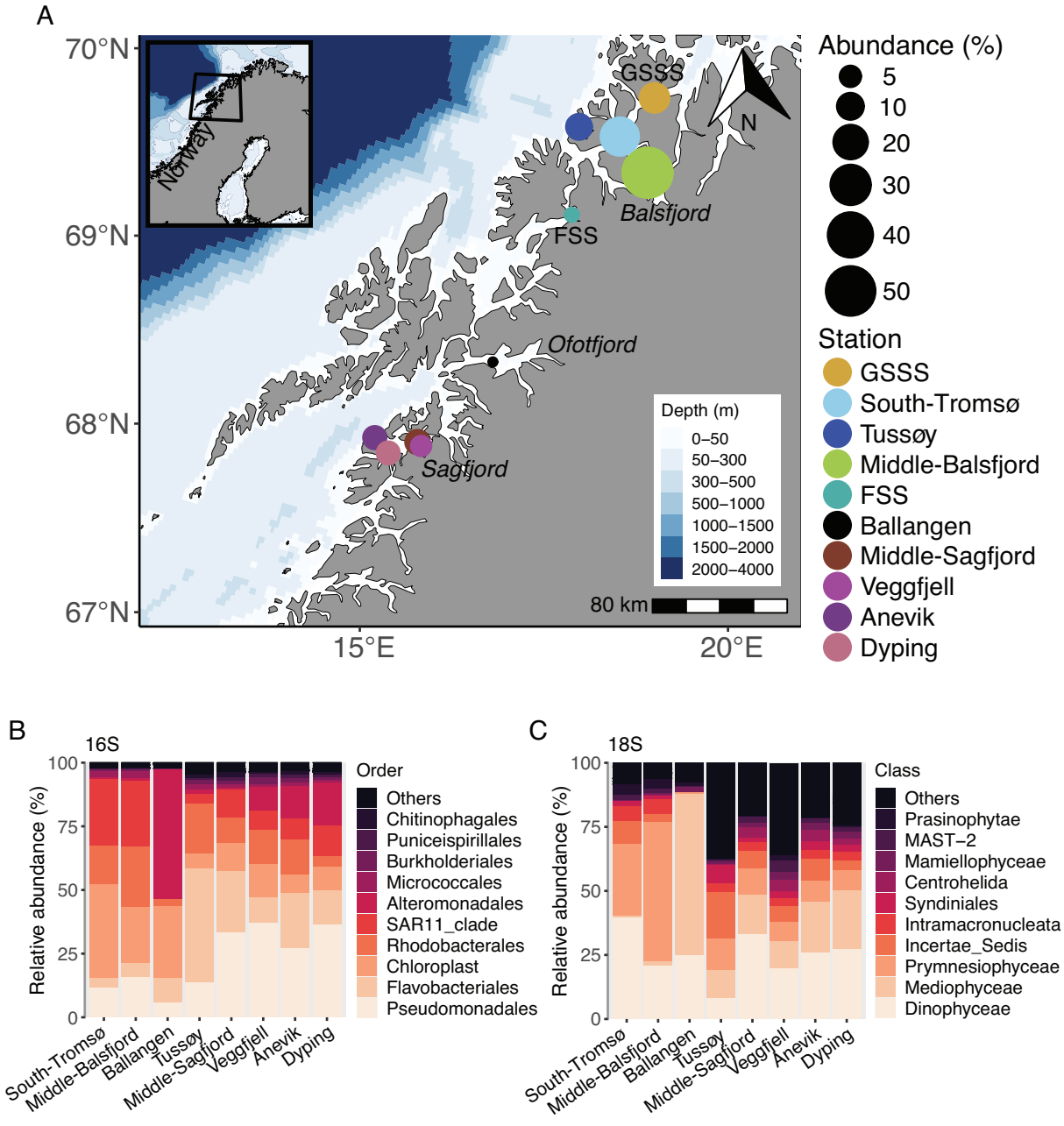


**Figure 1.** A map showing the geographical area in northern Norway where *Chrysochromulina leadbeateri* -related harmful algal bloom occurred in summer 2019. The main sample locations are *named* on the map. **A)** Microbial DNA for 18S rRNA and 16S rRNA amplicon sequence

analysis was collected once from the marked stations, except from FSS (Finnfjord sampling station) and GSSS (Grøtsund sampling station) which are the primary stations of this time series study and were sampled 7 and 8 times, respectively, between May 27th and June 21st. The size of the circles represents the relative abundance of focal taxon (average relative abundance for FSS and GSSS stations across all samples). Not all of the stations represent localities where HAB- related fish mortality was experienced. Taxonomic composition of the most abundant **B)** prokaryotes (16S) and **C)** microeukaryotes (18S) retrieved from Amplicon Sequence Variants (ASVs) tables specified at the order and class taxonomic rank level, respectively. Note that FSS and GSSS stations are excluded from **B** and **C** as the taxonomic composition across time series is shown in Figure 2.

**Microbiome dynamics across the bloom.** The microeukaryotic and prokaryotic community composition changed across the time series sampling campaign at FSS (PERMANOVA: 16S, $R^2 = 0.11$ and $p = 0.001$; 18S, $R^2 = 0.19$ and $p = 0.001$) and GSSS (PERMANOVA: 16S, $R^2 = 0.13$ and $p = 0.001$; 18S, $R^2 = 0.13$ and $p = 0.001$). These dynamic communities were also significantly dissimilar between the two time series stations (PERMANOVA: 16S, $R^2 = 0.30$ and $p = 0.001$; 18S, $R^2 = 0.46$ and $p = 0.001$) (Supplementary Table S3). GSSS showed higher species richness as compared to FSS as measured by the number of observed ASVs per sample day; 235–288 and 244–358 ASVs for 16S and accordingly 161–265 and 306–415 ASVs for 18S in FSS and GSSS, respectively (Supplementary Figure S6).

Among the most abundant microeukaryotes assigned to the taxonomic level class, only 18S ASVs indicative of *Cryptophyceae*, *Mediophyceae*, *Dinophyceae* and *Prymensiophyceae* (including the focal taxon) were shared between both stations (Figure 2a-b). The observed community in FSS was dominated by taxa classified as *Cryptophyceae* (9 – 49 % of the relative abundance), comprising mainly ASVs assigned to the genus *Teleaulax*, that showed strong temporal variability in the second half of the time series (Figure 2a and Supplementary Data S4 (osf.io)). The predominant taxon observed from GSSS was classified as *Dinophyceae,* which accounted for 34–54 % of the relative abundance during the time series (Figure 2b). Most of the ASVs belonging to the class *Dinophyceae* were not assigned to a lower taxonomic level.

338 A change in community structure was observed at both stations during the middle of the
339 observed bloom; between days 7 and 15 in FSS and between days 11 and 16 at the GSSS station
340 (Figure 2a-b). This shift was observed with an increased relative abundance of ASVs indicative
341 of centric diatoms (class *Mediophyceae*) in both stations and the class *Coscinodiscophytina* in
342 FSS which were almost exclusively represented by ASVs indicative within genus
343 *Leptocylindru*s (Figure 2a-b and Supplementary Data S4). The class *Mediophyceae* comprised
344 ASVs that were classified within different genera between stations, such as *Acrocellulus* at FSS
345 and *Thalassiosira* at GSSS (Supplementary Data S4-S5 (osf.io)). In FSS, the contribution of
346 class *Prymnesiophyceae* to the community composition was minor in comparison to GSSS
347 (Figure 2a-b) and was composed mainly by ASVs classified to the genus *Chrysochromulina* (2
348 – 3 % of relative abundance) but also ASVs assigned to the focal taxon, OLI16029 (0.5 – 1 %
349 of relative abundance) (Figure 2c and Supplementary Data S4-S5 (osf.io)). In GSSS, class
350 *Prymnesiophyceae* prevailed until day 11 (42 % of the relative abundance) and thereafter
351 drastically decreased while ASVs assigned to *Syndiniales* concurrently increased (Figure 2b).
352 The majority of those ASVs belonging to the class *Prymnesiophyceae* were assigned to the
353 genera *Phaeocystis* and the focal taxon (OLI16029) (Supplementary Data S5 (osf.io)). The
354 pronounced decrease in abundance of the focal taxon at day 8 coincided with highest relative
355 abundance of *Phaeocystis* (Figure 2d and Supplementary Data S5 (osf.io)). We note here for
356 clarity that ASVs assigned to the genus *Chrysochromulina* are not indicative of the focal taxon
357 (OLI16029), even though the unialgal control has been deposited and frequently referred to as
358 *Chrysochromulina leadbeateri* UiO-035.

359 The 16S ASVs – classified at the level of order – showed less temporal variability than
360 the 18S ASVs (at the class level) across the time series in FSS and GSSS. The taxa with the
361 highest relative abundances were the same in FSS and GSSS sample stations (Figure 2e-f).
362 Taxa classified to the order *Flavobacteriales* showed the highest relative abundance with ASVs

363 belonging *Rhodobacterales* and *Pseudomonadales* being common as well in both time series
364 stations (Figure 2e-f). The FSS and GSSS locations harbored distinctly different relative
365 abundances of genera assigned to *Flavobacteriales*. At station GSSS, the dominant genera were
366 *Polaribacter*, *Ulvibacter*, *Formosa* and the NS5 marine group, as compared to FSS where the
367 NS5 and NS9 marine groups were dominant (Supplementary Data S6 and S7 (osf.io)). At
368 GSSS, members of the order *Verrumicrobiales* increased in relative abundance (from 1 % to 8
369 %**)** within the same time frame as major changes in the microeukaryotes were observed (Figure
370 2f). Also, the abundance of the *Pseudomonadales* order decreased towards the end of the time
371 series while the contribution of *Flavobacteriales* simultaneously increased (Figure 2f). The
372 influence of Archaea to the 16S ASV composition was minor at both stations and accounted
373 for only 0.1 % and 0.4 % of the relative abundance in FSS and GSSS, respectively
374 (Supplementary Data S6 and S7 (osf.io)).
375 Since this study did not include measurements of chlorophyll *a* to indicate changes in
376 phytoplankton abundance, the 16S ASVs identified as Chloroplast were used as an inference.
377 The average relative abundance of ASVs assigned to Chloroplast was nearly three times higher
378 in FSS than in GSSS and the temporal pattern was different: the abundance increased towards
379 the end of the time series in FSS whereas in GSSS this was opposite (Figure 2e-f).
380

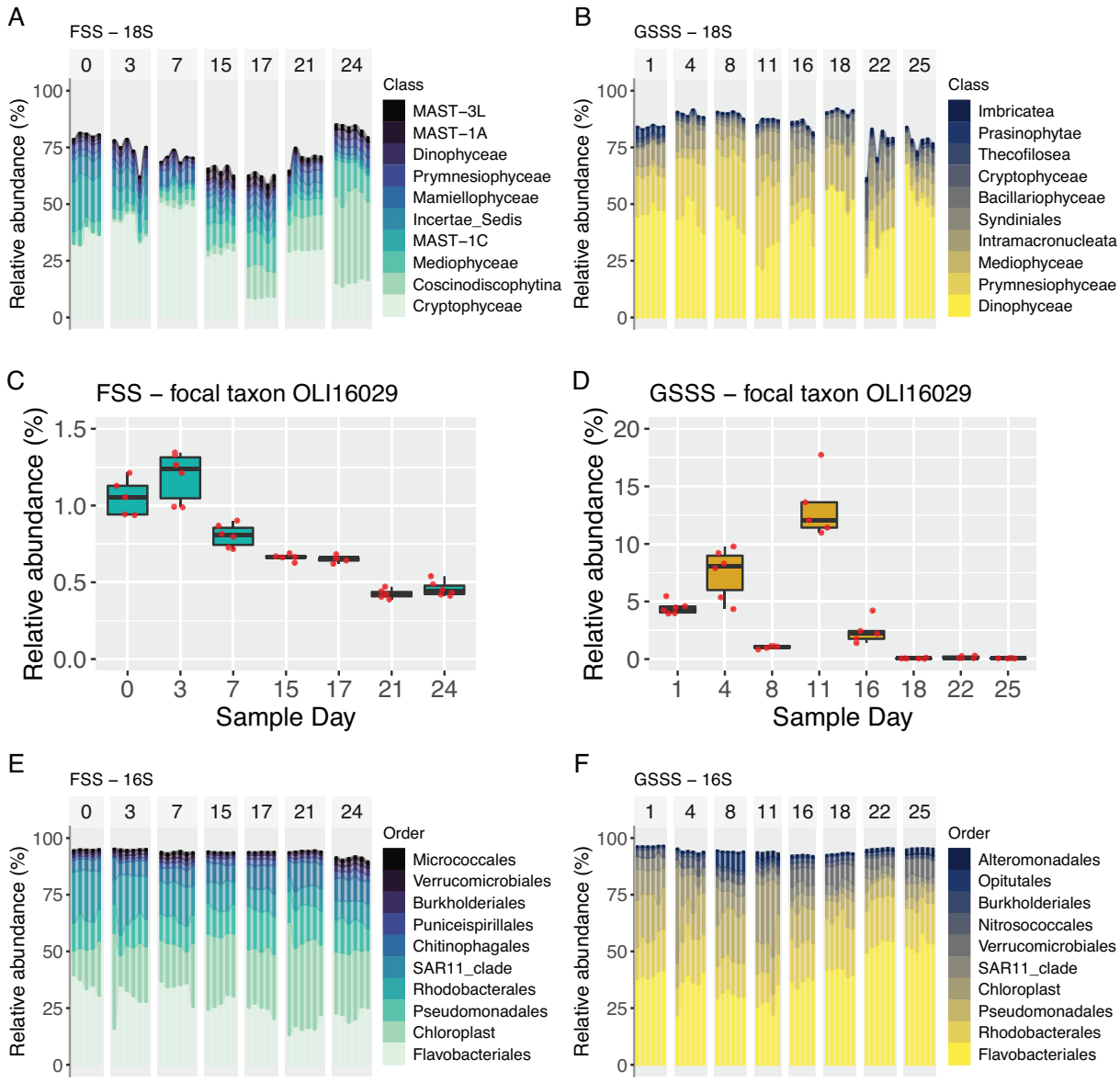


**Figure 2.** Comparative composition of the most common microeukaryotic and prokaryotic taxa collected from the time series sample stations and determined via 16S and 18S rRNA amplicon analysis. Microeukaryotes classified at the class taxonomic rank level **A**) in FSS and **B**) in GSSS. The temporal change in relative abundance of the focal taxon assigned as genus *OLI16029* (class *Prymnesiophyceae*) **C)** in FSS and **D)** in GSSS. Prokaryotes classified at the order taxonomic rank level **E)** in FSS and **F)** in GSSS.

**Environmental variability during the HAB**. The surface water properties – temperature and salinity – were relatively similar during the HAB, as observed from both time series stations (FSS and GSSS) at 10 m depth from where microbial biomass was collected (Supplementary Table S4). The overlaying surface water was more stratified in FSS than GSSS. This was due

393 to a low salinity layer (< 30) which persisted near the surface during the entire time series
394 simultaneously with a strong increase in observed temperature (Supplementary Figure S1 and
395 S2). The mixed layer depth was observed near the surface (3 m) throughout the study period in
396 FSS and in the beginning in GSSS time series, where it then sank down to 7 m by the end of
397 the GSSS time series while the surface water became more homogeneous after day 8
398 (Supplementary Figure S1 and S2). The mean $NO_3^-$ + $NO_2^-$ concentration was significantly
399 higher in GSSS than in FSS (0.43 and 0.18 μmol $L^{-1}$, respectively; Tukey, $p < 0.02$) whereas
400 the $Si(OH)_4$ and $PO_4^{3-}$ concentrations did not show statistically significant differences between
401 stations (Supplementary Table S4).
402
403 **Beta diversity in context with the environment**. Both the microeukarytotic and prokarytotic
404 components of the HAB-associated microbiome were dissimilar between GSSS and FSS
405 stations and throughout the observed time series. This was measured via unweighted UniFrac
406 distances that were ordinated by dbRDA analysis to infer the correlation between selected
407 environmental measurements to differences in community composition (Figure 3). Results of
408 beta diversity also corroborated the observed change in community structure during the middle
409 of the time series that was seen and noted above by inspecting changes in relative taxonomic
410 abundance (Figure 2). The dbRDA analysis (i.e., sum of RDA1 and RDA2) showed that 77.9
411 % and 83.7 % of the total variation in the prokaryotic and microeukaryotic community
412 composition was correlated to environmental measurements during the time series (Figure 3).
413 Most of this variation was explained by the first RDA component (RDA1: 16S = 60.8 % and
414 18S = 72.6 %) inferring that the variation of both prokaryotic and microeukaryotic communities
415 between FSS and GSSS may be driven by response to environmental factors such as MLD,
416 salinity, and $NO_3^-$ + $NO_2^-$ (Figure 3). Whereas the temporal variability within stations was

417 mainly explained by the second RDA component (RDA2) which accounted for 17.1 % and 11.1

418 % of the variance in prokaryotic and microeukaryotic communities, respectively.

419

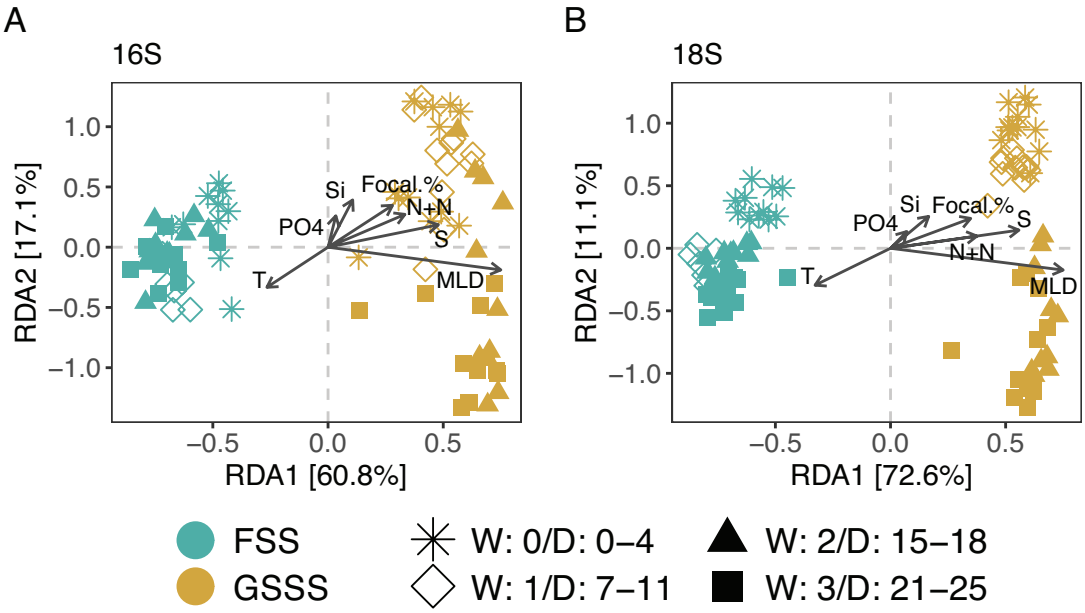


420

421 **Figure 3.** Dissimilarity in prokaryotic and microeukaryotic community composition between
422 sample stations was inferred via beta-diversity as measured with unweighted UniFrac distances
423 and related to environmental measurements. Distance-based redundancy analysis (dbRDA)
424 biplot of **A)** prokaryotes and **B)** microeukaryotes. Color represents station and shape comprises
425 samples (sample scores) within each sample week according to legend information. Arrows
426 indicate environmental factors and point to the direction of maximum variation of the respective
427 factor. T, temperature; S, salinity; MLD, mixed layer depth, Si, $Si(OH)_4$; PO4, $PO_4^{3-}$; N+N,
428 $NO_2^- + NO_3^-$; Focal %, relative abundance of focal taxon in 18S data set.

429

430 **Temporal trends and co-blooming taxa.** The HAB-associated marine microbiome was

431 complex and consisted of a minimum of 235 and 161 16S and 18S ASVs, respectively, each

432 maintaining its own dynamic trajectory during the observed time series. Examination and

433 subsequent clustering of the most predominant blooming patterns was performed via the k-

434 medoids clustering method. The resulted number of clusters per data set and time series station,

435 as assessed via the Calinski-Harabasz index (normalized ratio for inter-intra-cluster variance)

436 (Supplementary Figure S5), was 3, except for 18S at FSS where 4 clusters were selected. The

437 temporal pattern of each cluster was specified by its medoid taxon as a representative shape for
438 cluster's blooming dynamics of microeukaryotes (Figure 4a-b) and co-blooming taxa assigned
439 to 16S ASVs (Figure 5a-b).

440 The medoid 18S taxon of cluster 1 and 3, from both stations, exhibited approximately
441 inverse blooming patterns. These clusters also showed strong fluctuation in relative abundances
442 across the time series, including a strong positive and negative shift, respectively, around the
443 middle time points and negative correlations to environmental measurements (Figure 4a-d).
444 The medoid taxon of cluster 2 and 4 in FSS and cluster 2 in GSSS exhibited a short increase in
445 abundance in the beginning or end of time series (Figure 4a-b).

446 The focal ASV was included within cluster 3, at both stations (Figure 4a-b). There were
447 several microalgae that co-bloomed with the focal ASV, but these were distinct between the
448 FSS and GSSS stations (Figure 4). In FSS the focal ASV co-bloomed with genera *Teleaulax*
449 (class *Cryptophyceae*) and *Leptocylindrus* (class *Coscinodiscophytina*) which comprised 16 –
450 53 % and 1 – 53 % of the relative abundance within their respective cluster 3 (Figure 4e and
451 Supplementary Data S8 (osf.io)). A diverse composition of ASVs indicative of MAST clades
452 (marine stramenopiles) were also detected, although their relative abundances were minor (< 1
453 % of relative abundance within the cluster 3). This group was represented with other nano- and
454 picoplankton such as genera *Telonema* (class *Insertea Sedis*) and *Picomonas* (class
455 *Picomonadida*) the taxa in cluster 1 with inverse blooming pattern to cluster 3 (Figure 4c,e and
456 Supplementary Data S9 (osf.io)). ASVs from the genus *Phaeocystis* predominantly co-bloomed
457 at GSSS with the focal ASV (within cluster 3) together with a less abundant group of ciliates
458 (class *Intramacronucleata*) and members belonging to genus *Thalassiosira* (class
459 *Mediophyceae*) (Figure 4d,f and Supplementary Data S10 (osf.io)). ASVs belonging to the class
460 *Dinophyceae* also included in cluster 3 from GSSS (along with the focal ASV), and these were
461 composed mainly of members classified within the genus indicative of *Gymnodinium*.

The blooming patterns of 16S ASVs were also clustered. Among these, two clusters (1 and 2 from FSS and GSSS, respectively) showed significant positive correlation (FSS: $r = 0.79$ , $p = 0.036$ and GSSS: $r = 0.71$, $p = 0.047$) with the focal ASV. Only cluster 2 from station FSS showed a significant negative correlation with the focal ASV ($r = -0.96$, $p < 0.001$) (Figure 5c-d). The temporal trend represented by the medoid taxon was nearly identical in cluster 3 at both stations corresponding to the blooming pattern of cluster 2 and inverse blooming pattern of cluster 4 for microeukaryotes in GSSS and FSS, respectively.

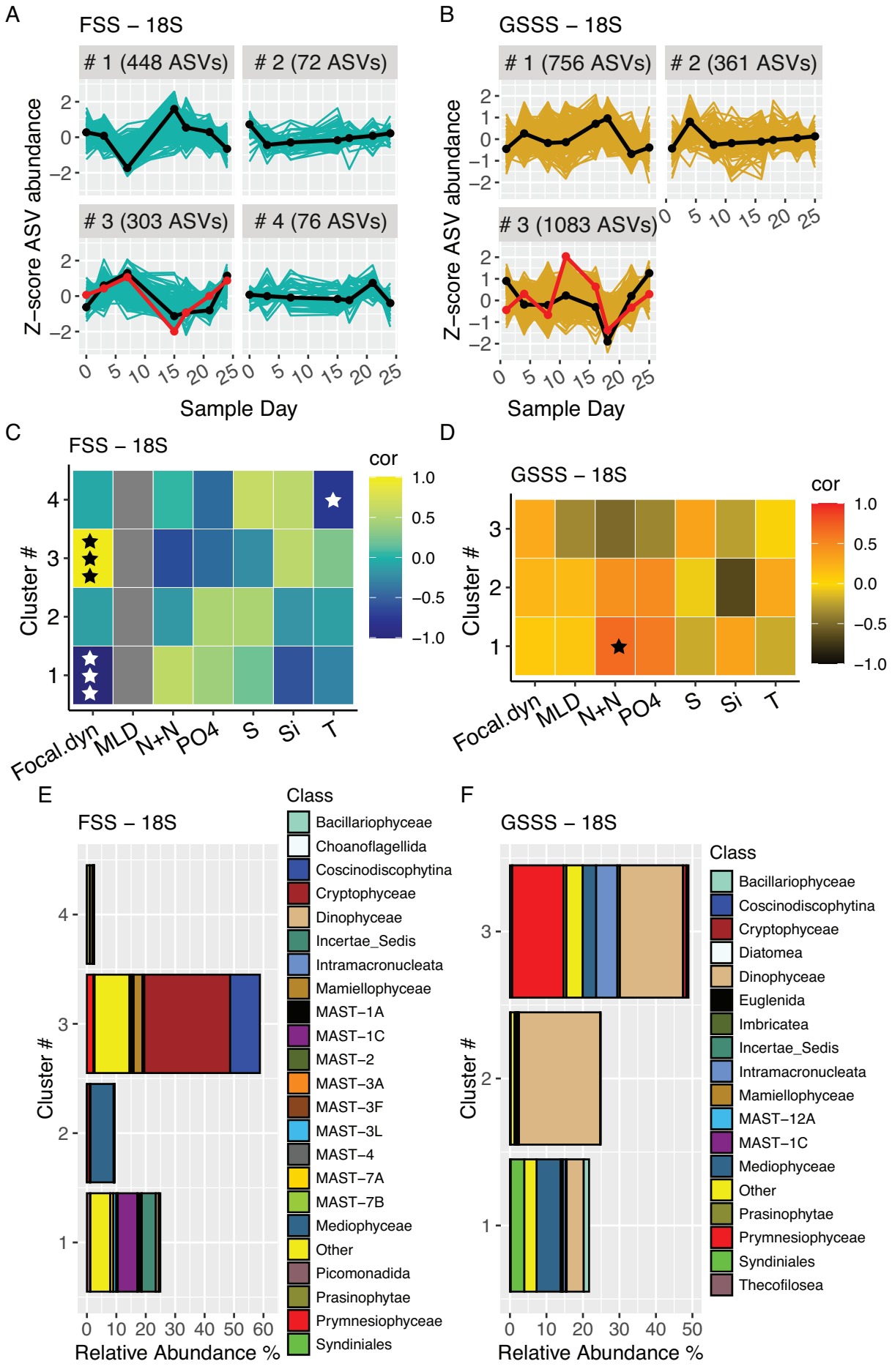
A
FSS – 18S
# 1 (448 ASVs)
# 2 (72 ASVs)
# 3 (303 ASVs)
# 4 (76 ASVs)
Z−score ASV abundance
Sample Day
B
GSSS – 18S
# 1 (756 ASVs)
# 2 (361 ASVs)
# 3 (1083 ASVs)
Z−score ASV abundance
Sample Day
C
FSS – 18S
Cluster #
cor
Focal.dyn
MLD
N+N
PO4
S
Si
T
D
GSSS – 18S
Cluster #
cor
Focal.dyn
MLD
N+N
PO4
S
Si
T
E
FSS – 18S
Cluster #
Relative Abundance %
Class
Bacillariophyceae
Choanoflagellida
Coscinodiscophytina
Cryptophyceae
Dinophyceae
Incertae_Sedis
Intramacronucleata
Mamiellophyceae
MAST−1A
MAST−1C
MAST−2
MAST−3A
MAST−3F
MAST−3L
MAST−4
MAST−7A
MAST−7B
Mediophyceae
Other
Picomonadida
Prasinophytae
Prymnesiophyceae
Syndiniales
F
GSSS – 18S
Cluster #
Relative Abundance %
Class
Bacillariophyceae
Coscinodiscophytina
Cryptophyceae
Diatomea
Dinophyceae
Euglenida
Imbricatea
Incertae_Sedis
Intramacronucleata
Mamiellophyceae
MAST−12A
MAST−1C
Mediophyceae
Other
Prasinophytae
Prymnesiophyceae
Syndiniales
Thecofilosea

470

**Figure 4.** Characterization of major blooming patterns in microeukaryotic communities assessed by K-medoid clustering analysis with z-transformation and detrending of 18S ASVs. Temporal dynamics of microeukaryotic taxa and number of ASVs per defined cluster **A)** in FSS and **B)** in GSSS station. The blooming pattern of each cluster is specified by medoid taxon and drawn with black line. The red line specifies the blooming pattern of focal ASV. Y-axis is a z-score and a value 0 denotes the mean abundance. Heatmap of Pearson's correlation between temporal dynamics of medoid taxon (z-scores) of each cluster and focal ASV (z-scores) and environmental factors **C)** in FSS and **D)** in GSSS. Color indicates Pearson's correlation coefficient according to the color legend and level of significance is marked with ★ (★, $p \leq 0.1$; ★★, $p \leq 0.05$; ★ ★ ★, $p \leq 0.001$). The grey color for MLD in FSS denotes undefined correlation as MLD values remained the same through the study period. Focal.dyn, temporal dynamic of focal ASV; MLD, mixed layer depth; N+N, $NO_2^- + NO_3^-$; PO4, $PO_4^{3-}$; S, salinity; Si, $Si(OH)_4$; T, temperature. Taxonomic profile of the most common microeukaryotes of each cluster as relative abundance in a whole community classified at the class taxonomic rank level **E)** in FSS **F)** in GSSS.

We infer that the bacterial taxa from the GSSS station belonging to cluster 2 co-bloomed with phototrophic protists in general, because the ASVs assigned to Chloroplasts occupied the same cluster (Figure 5f and Figure 4f). This cluster was also the only one to show a statistically significant correlation with phosphate concentrations. The same pattern was not observed in FSS where approximately two thirds of Chloroplast ASVs were identified within cluster 2 and rest in cluster 3 (Figure 5e).

Pearson correlation enabled us to infer that different bacterial taxa co-bloomed with the focal ASV at each time series sampling stations, FSS and GSSS (Figure 5c-d) corresponding to the observations within 18S microeukaryotes. Cluster 1 at station FSS was dominated by the order *Flavobacteriales* (35 – 63 % relative abundance within cluster 1) (Figure 5e) and was predominated by sequences identified within the NS5 marine group but also *Ulvibacter* (Supplementary Data S11 (osf.io)). ASVs assigned to *Rhodobacterales*, notably evenly dominating genera *Amylibacter* and *Planktomarina*, also shared the similar temporal dynamics with the focal ASV (Figure 5e and Supplementary Data S11 (osf.io)). The positive co-blooming trend between *Flavobacteriales* and *Rhodobacterales* classes and the focal ASV was not observed at station GSSS.

503

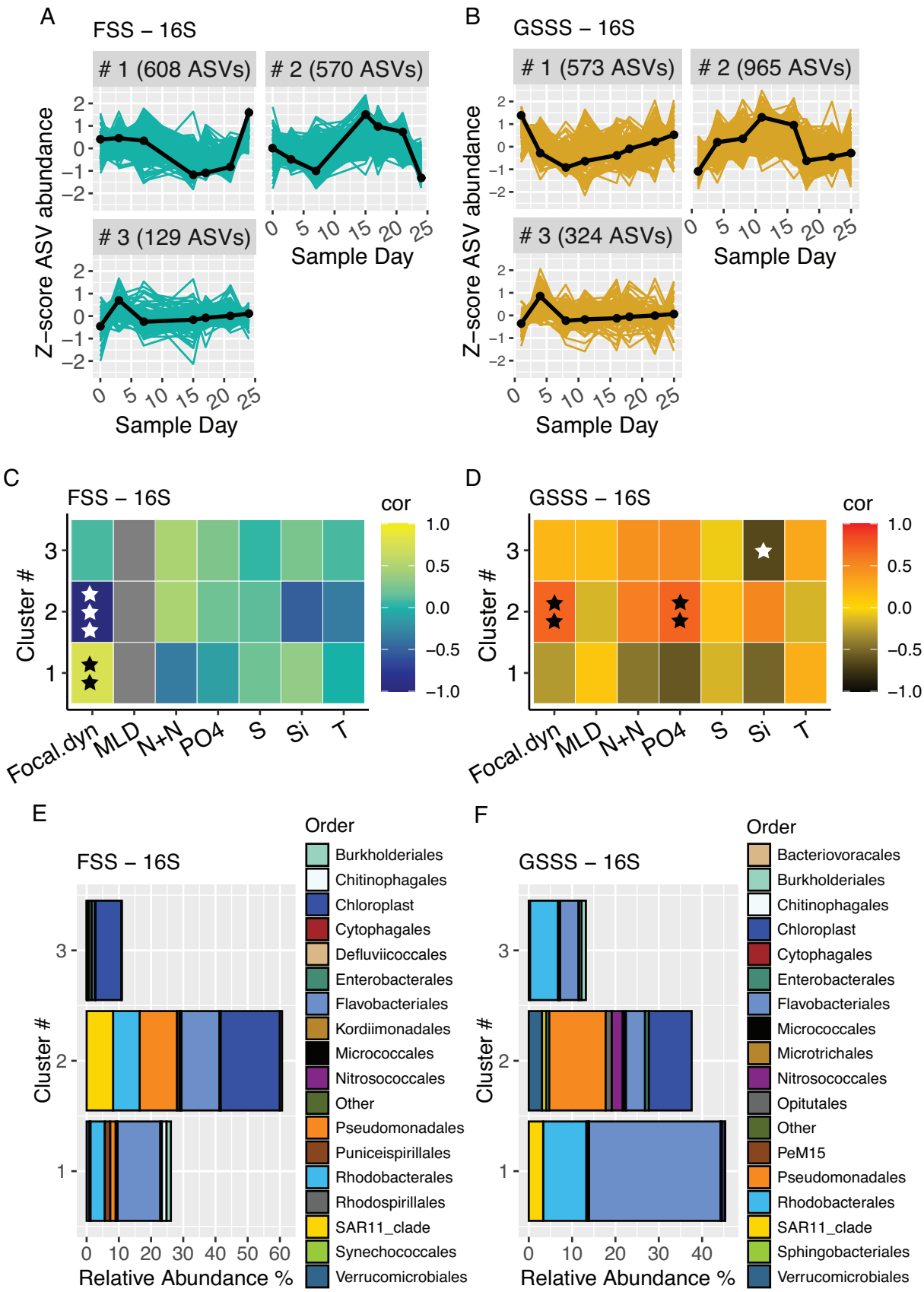
A
FSS – 16S
# 1 (608 ASVs)
# 2 (570 ASVs)
# 3 (129 ASVs)
Z−score ASV abundance
Sample Day
B
GSSS – 16S
# 1 (573 ASVs)
# 2 (965 ASVs)
# 3 (324 ASVs)
Z−score ASV abundance
Sample Day
C
FSS – 16S
Cluster #
Focal.dyn
MLD
N+N
PO4
S
Si
T
cor
D
GSSS – 16S
Cluster #
Focal.dyn
MLD
N+N
PO4
S
Si
T
cor
E
FSS – 16S
Cluster #
Relative Abundance %
Order
Burkholderiales
Chitinophagales
Chloroplast
Cytophagales
Defluviicoccales
Enterobacterales
Flavobacteriales
Kordiimonadales
Micrococcales
Nitrosococcales
Other
Pseudomonadales
Puniceispirillales
Rhodobacterales
Rhodospirillales
SAR11_clade
Synechococcales
Verrucomicrobiales
F
GSSS – 16S
Cluster #
Relative Abundance %
Order
Bacteriovoracales
Burkholderiales
Chitinophagales
Chloroplast
Cytophagales
Enterobacterales
Flavobacteriales
Micrococcales
Microtrichales
Nitrosococcales
Opitutales
Other
PeM15
Pseudomonadales
Rhodobacterales
SAR11_clade
Sphingobacteriales
Verrucomicrobiales

504

**Figure 5.** Characterization of major blooming patterns in prokaryotic communities assessed by K-medoid clustering analysis with z-transformation and detrending of 16S ASVs. Temporal dynamics of microeukaryotic taxa and number of ASVs per defined cluster **A)** in FSS and **B)** in GSSS station. The blooming pattern of each cluster is specified by medoid taxon and drawn with black line. Y-axis is a z-score and a value 0 denotes the mean abundance. Heatmap of Pearson's correlation between temporal dynamics of medoid taxon (z-scores) of each cluster and focal ASV (z-scores; Figure 4) and environmental factors **C)** in FSS and **D)** in GSSS. Color indicates Pearson's correlation coefficient according to the color legend and level of significance is marked with ★ (★, $p \leq 0.1$; ★★, $p \leq 0.05$; ★ ★ ★, $p \leq 0.001$). The grey color for MLD in FSS denotes undefined correlation as MLD values remained the same through the study period. Focal.dyn, temporal dynamic of focal ASV; MLD, mixed layer depth; N+N, $NO_2^-$ + $NO_3^-$; PO4, $PO_4^{3-}$; S, salinity; Si, $Si(OH)_4$; T, temperature. Taxonomic profile of the most common prokaryotes of each cluster as relative abundance in a whole community classified at the class taxonomic rank level **E)** in FSS **F)** in GSSS.

## DISCUSSION

The results from this study show distinct spatial variation and differences in the dynamic community composition across the portion of the northern Norwegian coast that was strongly affected during the 2019 *Chrysochromulina leadbeateri* HAB. This was a major and disruptive event due to severe fish mortality and hence there were several sampling campaigns launched simultaneously by public and private stakeholders. To our knowledge, this study represents the only molecular-based investigation of the holistic marine microbiome during this HAB event.

### Indication for separate focal blooms.

The 2019 HAB was reported on and monitored daily with focus on afflicted fish farm localities by the Norwegian Directorate of Fisheries (Karlsen et al., 2019). The results obtained from our amplicon-based sequencing approach are expected to be more complex and distinct from the concurrent morphology-based taxonomy and cell counting surveys. However, our results share some reassuring similarities to other reports, such as the observation that high focal taxon (OLI16029 as representative ASVs for *C. leadbeateri* UiO-035 unialgal strain) abundance was found in Balsfjord, which corresponds with microscopy enumerations conducted by Institute of Marine Research and Akvaplan-Niva (Karlsen et al., 2019; Grann-Meyer, 2020). The current

537 study did not capture the onset of the HAB due to a reactive sampling effort to an event that is
538 (at least today) impossible to predict.

539 According to the prevailing consensus based on reported fish mortality, the toxic bloom
540 of the focal taxon initiated in Ofotfjord. The last report on fish mortality in Ofotfjord was dated
541 four days before the sample in Ballangen was taken (Karlsen et al., 2019), thus there was,
542 presumably, a mismatch between the bloom peak and time of sampling. We do not have data
543 that represents the community composition during the first reports of fish mortality. This may
544 explain why we found a surprising high disparity between expected and observed microbial
545 community composition at Ballangen, which did not correspond with any other sampled
546 microbial community composition (Figure 1). The microeukaryotic community was dominated
547 by diatoms, nearly exclusively composed by *Skeletonema*. A similar shift from *C. leadbeateri*
548 presence to absence with concurrent predominance of diatoms was observed during the 1991
549 HAB around Ofotfjord and surrounding areas (Hegseth and Eilertsen, 1991; Rey and Aure,
550 1991). Correspondingly, the sampled prokaryotic community composition in Ballangen does
551 not presumably represent either the situation with *C. leadbeateri* as a disruptive causative agent
552 as several genera belonging to the observed predominant bacterial order *Alteromonadales* have
553 been found to associate with *Skeletonema* sp. (Deng et al., 2021).

554 *C. leadbeateri* and presumably the cells assigned to the focal taxon in our sequencing
555 analysis are common and natural members of phytoplankton community along the entire
556 northern Norwegian coast, although its spatial and interannual variation has not been well
557 described since the 1991 HAB, as only two following years of monitoring was conducted in
558 area south and north from Ofotfjord (Hegseth and Eilertsen, 1991; Heidal and Mohus, 1995).
559 The present study, however, provides evidence for high spatial variation and non-cell-density-
560 dependent toxicity. As mentioned, the high abundance of our designated focal taxon in the
561 Balsfjord area was corroborated by manual cell counts and revealed by 18S rRNA amplicon

562 sequencing samples in this study (Figure 1). This was two weeks after the first reported fish
563 mortalities from Ofotfjord (Karlsen et al., 2019). Thus, this raises the question whether a bloom
564 of focal taxon commenced locally in Balsfjord. Due to limited connectivity, it is likely that *C.*
565 *leadbeateri* blooms developed independently in both fjords since its relative abundance was
566 low in FSS station (Figure 2c) and no afflicted fish farms were reported near the FSS station,
567 despite of the affect on fish farms in the area north of Ofotfjord (Karlsen et al., 2019).
568 Interestingly, despite high abundance of the focal taxon and effective advection-driven
569 dispersal of cells from the inner part of Balsfjord towards GSSS and Tussøya stations, only one
570 fish farm near Tussøya was afflicted. However, this farm experienced limited impacts, and its
571 relation to the HAB remained somewhat questionable (Karlsen et al., 2019). This observation
572 also lends some indications to the idea that there may have been at least two distinct
573 physiological states between these two *C. leadbeateri* blooms, and that only one of them was
574 "harmful".
575
576 **Localized microbial communities.**
577 One of the major questions that drove this study was to ask how the marine microbiome
578 composition compared across locations during the HAB time series. The results revealed
579 distinct communities between sample locations, each possessing different predominating
580 bacterial and eukaryotic microbial groups (Figure 1 and Figure 2). This observation on spatial
581 heterogeneity provides new information on the development of the late bloom phase within an
582 interconnected coastal area (Wassmann et al., 1996). GSSS was the only station where
583 *Phaeocystis* abundance exceeded that of the focal taxon. In fact, the relative abundance of
584 *Phaeocystis* was less than 1 % at all other stations, which was an unexpected result given
585 previously reported ubiquity and prolonged prevalence (March-August) in this region (Eilertsen
586 et al., 1981; Degerlund and Eilertsen, 2010).

587 Although the predominant microalgae groups found in the two time series stations were
588 different (FSS: cryptophytes, *Leptocylindrus*, heterotrophic nanoflagellates; GSSS;
589 dinoflagellates, prymnesiophyte, *Thalassiosira*), the most abundant bacterial taxa – i.e. orders
590 *Flavobacteriales*, *Rhodobacterales* and *Pseudomonadales* – were essentially consistent.
591 Previously reported studies have also shown that members belonging to these orders commonly
592 accompany microalgae in marine environments, except in the case of *Teleaulax* sp. and *C.*
593 *leadbeateri,* which may be due to lack of previous records from events such as the 1991 HAB
594 of northern Norway (Teeling et al., 2016; Ajani et al., 2018; Zhou et al., 2018; Aalto et al.,
595 2022). The bacterial community compositions obtained from Middle-Balsfjord and South-
596 Tromsø stations where distinct and corresponded to the highest observed relative abundance of
597 the focal taxon. Specifically, they harboured high relative abundances of SAR11 (mainly clade
598 Ia) and low contributions of *Flavobacteriales,* which is interesting given that SAR11 tend to be
599 negatively correlated with copiotrophic bacterial groups before and after the primary
600 phytoplankton bloom (Needham and Fuhrman, 2016; Teeling et al., 2016). However, the single
601 time point stations present a major limitation for interpreting the HAB microbiome, given that
602 the time series stations (FSS and GSSS) showed pronounced temporal variability during the
603 event.
604
605 **Temporal community dynamics.**
606 Another major aim of this study was to identify the temporal patterns of the HAB associated
607 microbiome and attempt to determine which taxa co-bloomed with the focal ASV. We found
608 that most of the microeukaryotic and bacterial taxa either co-bloomed or inversely co-bloomed
609 with the focal ASV – i.e. the clusters that showed significant positive or negative correlation
610 with the focal ASV also had the highest taxonomic richness (Figure 4 and Figure 5). There has
611 been evidence that the most abundant taxa undergo stronger shifts in their abundance than rare

612 taxa, which corresponds with our results where the most abundant bacterial orders and
613 microeukaryotic classes were mainly found within the clusters of highest temporal variability
614 (Lindh et al., 2015). However, the high number of taxa in these clusters is somewhat surprising
615 with regard of previous findings of highly coherent communities with well-defined groups of
616 interacting organisms (Martin-Platero et al., 2018). It is likely that the prescribed temporal
617 (sampling) resolution of this study was too coarse to capture the true frequency of taxonomic
618 turnover, which can be very fast (Needham and Fuhrman, 2016; Martin-Platero et al., 2018).
619 However, when an unpredicted and regionally large (250 km wide) HAB occurs, it poses major
620 logistical challenges to react quickly and access the sample locations with frequency that would
621 be the most optimal with biological perspective. The choice of optimal sampling locations is
622 also limited by immediate accessibility to sampling resources, such as suitable water craft.
623
624 **The environment.**
625 The third major question of this study was related to the abiotic environment and how it may
626 have influenced the microbiome composition and presence of the focal taxon. The HAB – as
627 inferred from relative abundance of the focal taxon – was stronger at GSSS than at FSS, yet it
628 occurred concurrently at both stations. The strong decrease in focal taxon abundance in the
629 middle of time series coincided, especially at GSSS, with a change in community composition.
630 However, this was evidenced poorly by environmental factors at both stations. Intriguingly,
631 these results are in accordance with previous findings suggesting lower importance of
632 continuous environmental factors such as temperature, inorganic nutrients and chlorophyll *a* on
633 a change in community composition after seasonal bloom initiation than biotic interactions
634 (Lindh et al., 2015; Needham and Fuhrman, 2016). Whereas, a strong periodical physical
635 forcing (wind, turbulence) can cause a change of entire community (Martin-Platero et al., 2018).
636 The measured water column properties did not indicate strong vertical mixing. However, the

surface water became somewhat more homogenous after the first week in the time series at GSSS as revealed from CTD-profiles (Supplementary Figure S2).

The difference in microeukaryotic composition between the two time series stations may be related to environmental factors as revealed by dbRDA analysis (Figure 3). The phosphate concentration was low at both stations and in addition the $NO_3^- + NO_2^-$ level was low in FSS, which potentially promoted the development of communities of heterotrophic and mixotrophic protists. Several MAST-clades (e.g., MAST-1C as dominant in FSS) are known to be bacterivores and *Teleaulax* has been determined to be mixotrophic, feeding heterotrophically on bacteria, thus relaxing the need for inorganic nutrients (Massana et al., 2006; Du Yoo et al., 2017). It is difficult to draw a link between nutrients and the focal taxon with the current data due to lack of nutrient measurements from stations with high focal taxon abundance such as Middle-Balsfjord and South-Tromsø. Despite the nutrient information, a plausible connection would be unlikely as even a 14-year survey in southern Norway on *Chrysochromulina* spp. cell and nutrients concentration did not provide a clear connection (Dahl et al., 2005). However, there are indications that *Chrysochromulina* spp. thrive in high N:P ratios during low phosphate concentration which potentially promotes toxicity if the condition becomes phosphate limited (Dahl et al., 2005; Edvardsen and Imai, 2006).

## CONCLUSION

A summary of investigations of the 1991 *Chrysochromulina leadbeateri* related harmful algal bloom in northern Norway writes that it would not have been possible to predict such an incident but it would be necessary to launch a coastal monitoring program (Rey, 1991). Three decades later, we fully agree with the latter statement. We certainly have a long way to go in order to predict how ecological principles underpin this sporadic event in a highly variable coastal area and it is difficult to get there by performing investigations that simply react to only

662 those blooms that have acute economic impacts. It is also difficult to plan to observe such a
663 bloom that happens so infrequently. It has become highly evident that this type of reoccurring
664 bloom is extremely destructive because it causes substantial losses for the fish farmers. In 1991
665 the fish kill damage linked to *C. leadbeateri* was 742 tonnes with a corresponding direct short
666 term economic cost of 3.5 million USD, while in 2019 these values were increased to 14 500
667 tonnes and more than 100 million USD (Karlson et al., 2021). Thus, it is expected these numbers
668 will become even higher in the future with increasing aquaculture industry, and there is no
669 reason to believe that this type of HAB will not reoccur. It is challenging to draw any
670 conclusions about exact causation behind the 2019 HAB, especially since the natural bloom
671 cycles of *C. leadbeateri* are not well understood. Therefore, this study relying on molecular-
672 based methods provides a first insight on the spatial and temporal variability of the *C.*
673 *leadbeateri*-like focal taxon together with its associated marine microbiome. It also supports
674 future molecular-based studies by providing a genetic link with currently available taxonomic
675 annotation between current and year 1991 *C. leadbeateri*. Otherwise the focal taxon may be
676 overlooked due to database limitations – an issue also present in this study. We found that most
677 of the taxa – including the most abundant members of prokaryotes and microeukaryotes and
678 the focal taxon – underwent strong and rapid variability in their succession dynamics. These
679 temporal dynamics were poorly connected to the environmental conditions measured,
680 suggesting that other factors such as biological interactions might drive the late bloom
681 dynamics.
682

683 **AUTHOR CONTRIBUTIONS**

684 NJA and HCB conceptualized the study. NJA, EG-M, JBS, LD, CJH and RI carried out the
685 sampling. NJA, HS, SK and SP performed lab work and processed amplicon sequence analyses.

NJA and HCB conducted data analysis and NJA wrote the manuscript draft. All authors contributed to the final version.

**ACKNOWLEDGMENTS**

We greatly appreciate the logistical support by staff at Lerøy Aurora´s aquaculture facility at Solheim. We also acknowledge the collaboration between Finnfjord AS and UiT-The Arctic University of Norway for lending sampling infrastructure and support. We would like thank Åge Mohus and Vigdis Tverberg at Nord University for their help with sample coordination in southern portion of the HAB affected area.

**FUNDING**

This study was funded directly by the Faculty of Biosciences, Fisheries and Economics at UiT – The Arctic University of Norway as the "2019 Harmful Algae Rapid Response Plan". The authors would like to specifically thank Terje Aspen, Terje Martinussen and Kathrine Tveiterås for providing rapid support and guidance.

**CONFLICT OF INTEREST**

The authors have no conflicts of interest to declare.

**REFERENCES CITED**

Aalto, N.J., Campbell, K., Eilertsen, H.C., and Bernstein, H.C. (2021). Drivers of atmosphere ocean CO2 flux in northern Norwegian fjords. *Frontiers in Marine Science*, 841. doi: 10.3389/fmars.2021.692093.

Aalto, N.J., Schweitzer, H., Krsmanovic, S., Campbell, K., and Bernstein, H.C. (2022). Diversity and selection of surface marine microbiomes in the Atlantic-influenced Arctic. *Frontiers in Microbiology*. doi: 10.3389/fmicb.2022.892634/abstract.

Abdi, H., and Williams, L.J. (2010). Tukey's honestly significant difference (HSD) test. *Encyclopedia of research design* 3(1), 1-5.

Ajani, P.A., Kahlke, T., Siboni, N., Carney, R., Murray, S.A., and Seymour, J.R. (2018). The Microbiome of the Cosmopolitan Diatom Leptocylindrus Reveals Significant Spatial

and Temporal Variability. *Frontiers in Microbiology* 9. doi: 10.3389/fmicb.2018.02758.

Amaral-Zettler, L.A., McCliment, E.A., Ducklow, H.W., and Huse, S.M. (2009). A method for studying protistan diversity using massively parallel sequencing of V9 hypervariable regions of small-subunit ribosomal RNA genes. *PloS one* 4(7)**,** e6372.

Anderson, D.M., Glibert, P.M., and Burkholder, J.M. (2002). Harmful algal blooms and eutrophication: nutrient sources, composition, and consequences. *Estuaries* 25(4)**,** 704-726.

Anderson, M.J. (2001). A new method for non-parametric multivariate analysis of variance. *Austral ecology* 26(1)**,** 32-46.

Caporaso, J.G., Kuczynski, J., Stombaugh, J., Bittinger, K., Bushman, F.D., Costello, E.K., et al. (2010). QIIME allows analysis of high-throughput community sequencing data. *Nat Methods* 7(5)**,** 335-336.

Cirri, E., and Pohnert, G. (2019). Algae− bacteria interactions that balance the planktonic microbiome. *New Phytologist* 223(1)**,** 100-106.

Coenen, A.R., Hu, S.K., Luo, E., Muratore, D., and Weitz, J.S. (2020). A primer for microbiome time-series analysis. *Frontiers in genetics* 11**,** 310.

Dahl, E., Bagøien, E., Edvardsen, B., and Stenseth, N.C. (2005). The dynamics of Chrysochromulina species in the Skagerrak in relation to environmental conditions. *Journal of Sea Research* 54(1)**,** 15-24.

Davidson, K., Gowen, R.J., Tett, P., Bresnan, E., Harrison, P.J., McKinney, A., et al. (2012). Harmful algal blooms: How strong is the evidence that nutrient ratios and forms influence their occurrence? *Estuarine, Coastal and Shelf Science* 115**,** 399-413. doi: https://doi.org/10.1016/j.ecss.2012.09.019.

Degerlund, M., and Eilertsen, H.C. (2010). Main species characteristics of phytoplankton spring blooms in NE Atlantic and Arctic waters (68–80 N). *Estuaries and coasts* 33(2)**,** 242-269.

Deng, Z., Chen, S., Zhang, P., Zhang, X., Adams, J.M., Luo, Q., et al. (2021). Dynamics of Free-Living and Attached Bacterial Assemblages in Skeletonema sp. Diatom Cultures at Elevated Temperatures. *Frontiers in Marine Science* 8. doi: 10.3389/fmars.2021.626207.

Doucette, G.J., McGovern, E.R., and Babinchak, J.A. (1999). ALGICIDAL BACTERIA ACTIVE AGAINST GYMNODINIUM BREVE (DINOPHYCEAE). I. BACTERIAL ISOLATION AND CHARACTERIZATION OF KILLING ACTIVITY1, 3. *Journal of Phycology* 35(6)**,** 1447-1454.

Du Yoo, Y., Seong, K.A., Jeong, H.J., Yih, W., Rho, J.-R., Nam, S.W., et al. (2017). Mixotrophy in the marine red-tide cryptophyte Teleaulax amphioxeia and ingestion and grazing impact of cryptophytes on natural populations of bacteria in Korean coastal waters. *Harmful Algae* 68**,** 105-117.

Edvardsen, B., Eikrem, W., Throndsen, J., Saez, A.G., Probert, I., and Medlin, L.K. (2011). Ribosomal DNA phylogenies and a morphological revision provide the basis for a revised taxonomy of the Prymnesiales (Haptophyta). *European journal of phycology* 46(3)**,** 202-228.

Edvardsen, B., and Imai, I. (2006). "The ecology of harmful flagellates within Prymnesiophyceae and Raphidophyceae," in *Ecology of harmful algae*. Springer), 67-79.

Edvardsen, B., and Paasche, E. (1998). Bloom dynamics and physiology of Prymnesium and Chrysochromulina. *NATO ASI SERIES G ECOLOGICAL SCIENCES* 41**,** 193-208.

Eikrem, W., and Throndsen, J. (1998). Morphology of Chrysochromulina leadbeateri (Prymnesiophyceae) from northern Norway. *Phycologia* 37(4)**,** 292-299.

Eilertsen, H.C., Falk-Petersen, S., Hopkins, C., and Tande, K. (1981). Ecological investigations on the plankton community of Balsfjorden, northern Norway: program for the project, study area, topography, and physical environment. *Sarsia* 66(1)**,** 25-34.

Eilertsen, H.C., and Frantzen, S. (2007). Phytoplankton from two sub-Arctic fjords in northern Norway 2002–2004: I. Seasonal variations in chlorophyll a and bloom dynamics. *Marine Biology Research* 3(5)**,** 319-332.

Eilertsen, H.C., and Taasen, J. (1984). Investigations on the plankton community of Balsfjorden, northern Norway. The phytoplankton 1976–1978. Environmental factors, dynamics of growth, and primary production. *Sarsia* 69(1)**,** 1-15.

Estep, K. (1984). Chloroplast containing microflagellates in natural populations of north Atlantic nanoplankton, their identification and distribution; including a description of 5 new species of Chrysochromulina (Prymnesiophyceae). *Protistologica* 20**,** 613-634.

Fuhrman, J.A., Cram, J.A., and Needham, D.M. (2015). Marine microbial community dynamics and their ecological interpretation. *Nature Reviews Microbiology* 13(3)**,** 133-146.

Gilbert, J.A., Meyer, F., Antonopoulos, D., Balaji, P., Brown, C.T., Brown, C.T., et al. (2010). Meeting report: the terabase metagenomics workshop and the vision of an Earth microbiome project. *Stand Genomic Sci* 3(3)**,** 243.

Grann-Meyer, E. (2020). *Chrysochromulina leadbeateri - Understanding the presumed causal agent behind the harmful algal bloom of 2019.* Master's thesis, UiT - Arctic University of Norway.

Green, D.H., Llewellyn, L.E., Negri, A.P., Blackburn, S.I., and Bolch, C.J. (2004). Phylogenetic and functional diversity of the cultivable bacterial community associated with the paralytic shellfish poisoning dinoflagellate Gymnodinium catenatum. *FEMS Microbiology Ecology* 47(3)**,** 345-357.

Guillard, R.R. (1975). "Culture of phytoplankton for feeding marine invertebrates," in *Culture of marine invertebrate animals*. Springer), 29-60.

Hallegraeff, G.M., Anderson, D.M., Belin, C., Bottein, M.-Y.D., Bresnan, E., Chinain, M., et al. (2021). Perceived global increase in algal blooms is attributable to intensified monitoring and emerging bloom impacts. *Communications Earth & Environment* 2(1)**,** 1-10.

Hegseth, E.N., and Eilertsen, H.C. (1991). The Chrysochromulina leadbeateri bloom in Troms May/June 1991. Development and causes. . *Fisk. Hav.* 3**,** 45-61.

Heidal, K., and Mohus, A. (1995). The toxic Chrysochromulina-- salmon disaster of 1991 in northern Norway with some follow-up monitoring records of 1992 and-93. *LAVOISIER, PARIS(FRANCE).* 163-168.

Karlsen, K.M., Robertsen, R., and Hersoug, B. (2019). Mapping the course of events and preparedness for algal blooms in spring 2019 - Astafjorden, Ofotfjorden, Vestfjorden og Tysfjorden. *Nofima AS* 29**,** 1-44.

Karlson, B., Andersen, P., Arneborg, L., Cembella, A., Eikrem, W., John, U., et al. (2021). Harmful algal blooms and their effects in coastal seas of Northern Europe. *Harmful Algae* 102**,** 101989.

Kaufman, L., and Rousseeuw, P.J. (2009). *Finding groups in data: an introduction to cluster analysis.* New York: John Wiley & Sons.

Lindh, M.V., Sjöstedt, J., Andersson, A.F., Baltar, F., Hugerth, L.W., Lundin, D., et al. (2015). Disentangling seasonal bacterioplankton population dynamics by high-frequency sampling. *Environmental microbiology* 17(7)**,** 2459-2476.

Liu, C., Cui, Y., Li, X., and Yao, M. (2021). microeco: an R package for data mining in microbial community ecology. *FEMS Microbiology Ecology* 97(2)**,** fiaa255.

Lord, E., Willems, M., Lapointe, F.-J., and Makarenkov, V. (2017). Using the stability of objects to determine the number of clusters in datasets. *Information Sciences* 393**,** 29-46.

Love, M.I., Huber, W., and Anders, S. (2014). Moderated estimation of fold change and dispersion for RNA-seq data with DESeq2. *Genome biology* 15(12)**,** 1-21.

Lozupone, C., Lladser, M.E., Knights, D., Stombaugh, J., and Knight, R. (2011). UniFrac: an effective distance metric for microbial community comparison. *The ISME journal* 5(2)**,** 169-172.

Martin-Platero, A.M., Cleary, B., Kauffman, K., Preheim, S.P., McGillicuddy, D.J., Alm, E.J., et al. (2018). High resolution time series reveals cohesive but short-lived communities in coastal plankton. *Nature communications* 9(1)**,** 1-11.

Massana, R., Terrado, R., Forn, I., Lovejoy, C., and Pedrós-Alió, C. (2006). Distribution and abundance of uncultured heterotrophic flagellates in the world oceans. *Environmental microbiology* 8(9)**,** 1515-1522.

Mayali, X., and Azam, F. (2004). Algicidal bacteria in the sea and their impact on algal blooms 1. *Journal of Eukaryotic Microbiology* 51(2)**,** 139-144.

Meldahl, A.S., Edvardsen, B., and Fonnum, F. (1994). Toxicity of four potentially ichthyotoxic marine phytoflagellates determined by four different test methods. *Journal of Toxicology and Environmental Health, Part A Current Issues* 42(3)**,** 289-301.

Meyer, N., Bigalke, A., Kaulfuß, A., and Pohnert, G. (2017). Strategies and ecological roles of algicidal bacteria. *FEMS Microbiology Reviews* 41(6)**,** 880-899.

Needham, D.M., and Fuhrman, J.A. (2016). Pronounced daily succession of phytoplankton, archaea and bacteria following a spring bloom. *Nature Microbiology* 1(4)**,** 16005. doi: 10.1038/nmicrobiol.2016.5.

Nielsen, T.G., Kiørboe, T., and Bjørnsen, P.K. (1990). Effects of a Chrysochromulina polylepis subsurface bloom on the planktonic community. *Marine Ecology Progress Series***,** 21-35.

Oksanen, J., Blanchet, F.G., Kindt, R., Legendre, P., Minchin, P.R., O'hara, R., et al. (2013). Package 'vegan'. *Community ecology package, version* 2(9).

Parte, A.C., Carbasse, J.S., Meier-Kolthoff, J.P., Reimer, L.C., and Göker, M. (2020). List of Prokaryotic names with Standing in Nomenclature (LPSN) moves to the DSMZ. *International Journal of Systematic and Evolutionary Microbiology* 70(11)**,** 5607.

Peralta-Ferriz, C., and Woodgate, R.A. (2015). Seasonal and interannual variability of pan-Arctic surface mixed layer properties from 1979 to 2012 from hydrographic data, and the dominance of stratification for multiyear mixed layer depth shoaling. *Progress in Oceanography* 134**,** 19-53.

R Core Team (2021). R: A language and environment for statistical computing, R Foundation for Statistical Computing.

Reigstad, M., and Wassmann, P. (1996). Importance of advection for pelagic-benthic coupling in north Norwegian fjords. *Sarsia* 80(4)**,** 245-257.

Rey, F. (1991). The Chrysochromulina leadbeateri bloom in Vestfjorden, north Norway, May-June 1991: Proceedings from a scientific working meeting. *Fisk. Hav.* 3**,** 1-122.

Rey, F., and Aure, J. (1991). The *Chrysochromulina leadbeateri* bloom in the Vestfjord, north Norway, May-June 1991. Environmental conditions and possible causes. *Fisk. Hav.* 3**,** 13-32.

Statistics Norway (2020). *Aquaculture 2019* [Online]. Statistics Norway. Available: https://www.ssb.no/jord-skog-jakt-og-fiskeri/statistikker/fiskeoppdrett [Accessed 23.04 2022].

Teeling, H., Fuchs, B.M., Bennke, C.M., Krueger, K., Chafee, M., Kappelmann, L., et al. (2016). Recurring patterns in bacterioplankton dynamics during coastal spring algae blooms. *elife* 5**,** e11888.

Uribe, P., and Espejo, R.T. (2003). Effect of associated bacteria on the growth and toxicity of Alexandrium catenella. *Applied and environmental microbiology* 69(1)**,** 659-662.

Uronen, P., Kuuppo, P., Legrand, C., and Tamminen, T. (2007). Allelopathic Effects of Toxic Haptophyte Prymnesium parvum Lead to Release of Dissolved Organic Carbon and Increase in Bacterial Biomass. *Microbial Ecology* 54(1)**,** 183-193. doi: 10.1007/s00248-006-9188-8.

Uronen, P., Lehtinen, S., Legrand, C., Kuuppo, P., and Tamminen, T. (2005). Haemolytic activity and allelopathy of the haptophyte Prymnesium parvum in nutrient-limited and balanced growth conditions. *Marine Ecology Progress Series* 299**,** 137-148.

Wassmann, P., Svendsen, H., Keck, A., and Reigstad, M. (1996). Selected aspects of the physical oceanography and particle fluxes in fjords of northern Norway. *Journal of Marine Systems* 8(1-2)**,** 53-71.

Zhou, J., Richlen, M.L., Sehein, T.R., Kulis, D.M., Anderson, D.M., and Cai, Z. (2018). Microbial Community Structure and Associations During a Marine Dinoflagellate Bloom. *Frontiers in Microbiology* 9. doi: 10.3389/fmicb.2018.01201.

893 **SUPPLEMENTARY MATERIAL**

894

895 **Microbial community dynamics during a harmful *Chrysochromulina leadbeateri* bloom**

896

897 Nerea J. Aalto[1,2], Hannah Schweitzer[1,2], Erlend Grann-Meyer[1], Stina Krsmanovic[1], Jon Brage

898 Svenning[1], Lars Dalheim[1], Sebastian Petters[1], Richard Ingebrigtsen[1], Chris J. Hulatt[3], Hans C.

899 Bernstein[1,2]*

900

901 **Affiliations:**

902 *1. Norwegian College of Fisheries Sciences, UiT - The Arctic University of Norway, Tromsø,*

903 *Norway*

904 *2. The Arctic Centre for Sustainable Energy, UiT - The Arctic University of Norway, Tromsø,*

905 *Norway*

906 *3. Faculty of Biosciences and Aquaculture, Nord University, Bodø, Norway*

907

908

909 ***Correspondence**: Hans C. Bernstein, UiT-The Arctic University of Norway, BFE-fak.,

910 Postboks 6050 Langnes, 9037 Tromsø, NORWAY*; Phone: +47 776 46 114; Email:*

911 Hans.C.Bernstein@uit.no

912

913

914

915

916

917

**Supplementary Table S1.** Station positions, sample dates, and corresponding sample day and week during time series sample campaign (May 27th = Sample day 0 and June 21st = Sample day 25).

| Station | Position | Sample date | Sample day/Sample week |
|---|---|---|---|
| FSS | 69.19 N, 18.03 E | 27.05.2019 | 0/0 |
| | | 30.05.2019 | 3/0 |
| | | 03.06.2019 | 7/1 |
| | | 11.06.2019 | 15/2 |
| | | 13.06.2019 | 17/2 |
| | | 17.06.2019 | 21/3 |
| | | 20.06.2019 | 24/3 |
| GSSS | 69.80 N, 19.36 E | 28.05.2019 | 1/0 |
| | | 31.05.2019 | 4/0 |
| | | 04.06.2019 | 8/1 |
| | | 07.06.2019 | 11/1 |
| | | 12.06.2019 | 16/2 |
| | | 14.06.2019 | 18/2 |
| | | 18.06.2019 | 22/2 |
| | | 21.06.2019 | 25/3 |
| South-Tromsø | 69.60 N, 18.80 E | 27.05.2019 | 0/0 |
| Middle-Balsfjord | 69.40 N, 19.20 E | 29.05.2019 | 2/0 |
| Tussøy | 69.66 N, 18.18 E | 06.06.2019 | 10/1 |
| Ballangen | 68.41 N, 16.83 E | 05.06.2019 | 9/1 |
| Middle-Sagfjord | 67.98 N, 15.75 E | 14.06.2019 | 18/2 |
| Veggfjell | 67.96 N, 15.80 E | 14.06.2019 | 18/2 |
| Anevik | 68.00 N, 15.14 E | 14.06.2019 | 18/2 |
| Dyping | 67.92 N, 15.34 E | 14.06.2019 | 18/2 |

**Supplementary Table S2.** The number of classified ASVs and sequencing depth per sample and data set before and after removal of unwanted taxa. Time series sample set includes stations FSS and GSSS; Single-time-point sample set includes stations Tussøya, South-Tromsø, Middle-Balsfjord, Ballangen, Middle-Sagfjord, Veggfjell, Anevik and Dyping; Unialgal control sample set includes *Chrysochromulina leadbeateri* UiO-035 strain culture.

| Condition | Sample set | Data set | # ASVs | Sample depth |
|---|---|---|---|---|
| All taxa | Time series | 16S | 2761 | 54160–217118 |
| | Time series | 18S | 7500 | 72831–34835 |
| | Single-time-point | 16S | 1414 | 83315–168168 |
| | Single-time-point | 18S | 3687 | 143296–469129 |
| | Unialgal control (UiO-035) | 18S | 123 | 134563–273163 |
| Removed unwanted taxa | Time series | 16S | 2644 | 53962–214722 |
| | Time series | 18S | 2674 | 56789–331887 |
| | Single-time-point | 16S | 1368 | 83253–167400 |
| | Single-time-point | 18S | 1682 | 118101–451910 |
| | Unialgal control (UiO-035) | 18S | 15 | 125686–265853 |

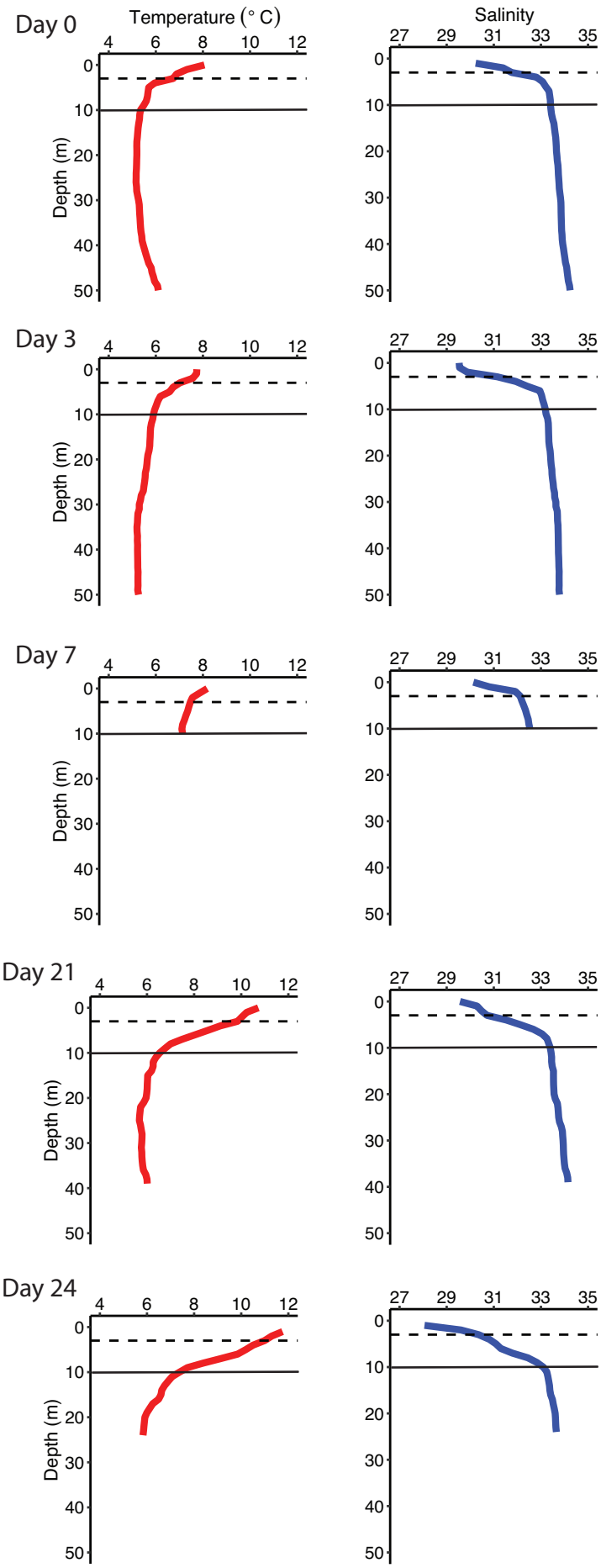


**Supplementary Figure S1.** Surface water profiles of temperature and salinity obtained from CTD-casts in FSS time series station. The dashed line denotes calculated mixed layer depth (MLD) based on density gradient and solid line marks the depth of sampled microbial communities (10 m). Note missing CTD-casts in sample days of 15 and 17.

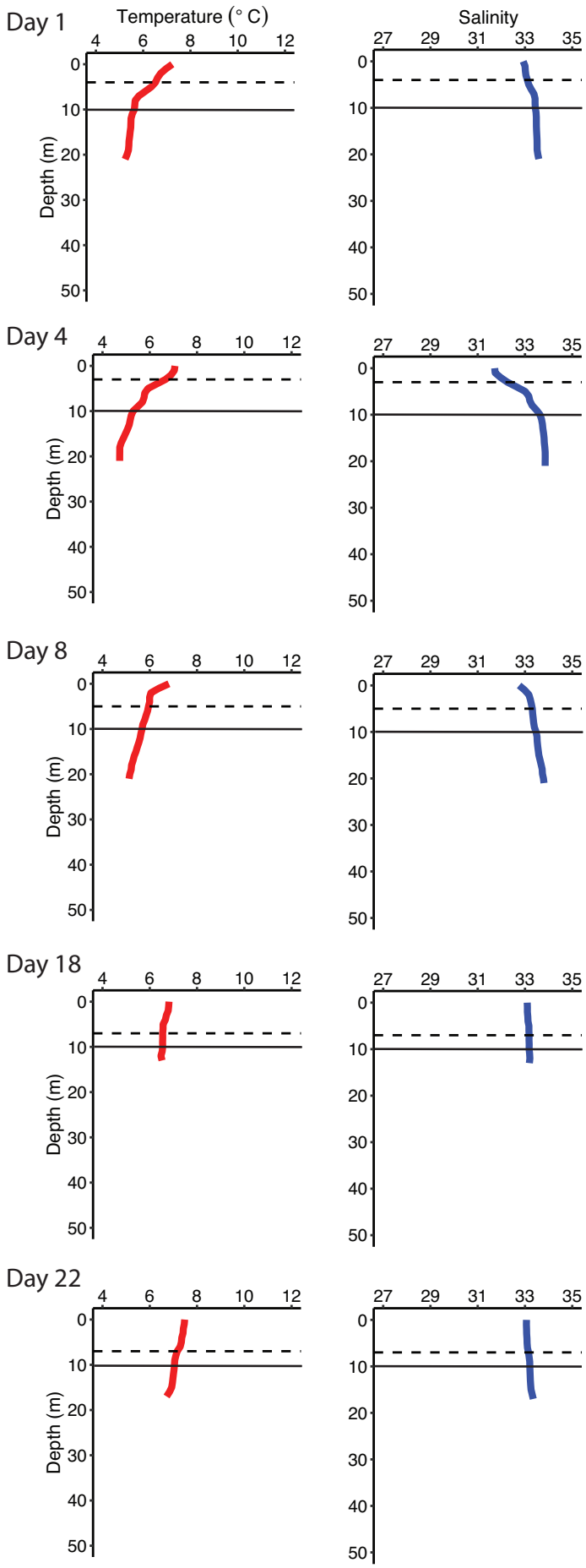


**Supplementary Figure S2.** Surface water profiles of temperature and salinity obtained from CTD-casts in GSSS time series station. The dashed line denotes calculated mixed layer depth (MLD) based on density gradient and solid line marks the depth of sampled microbial communities (10 m). Note missing CTD-casts in sample days of 11 and 16.

951

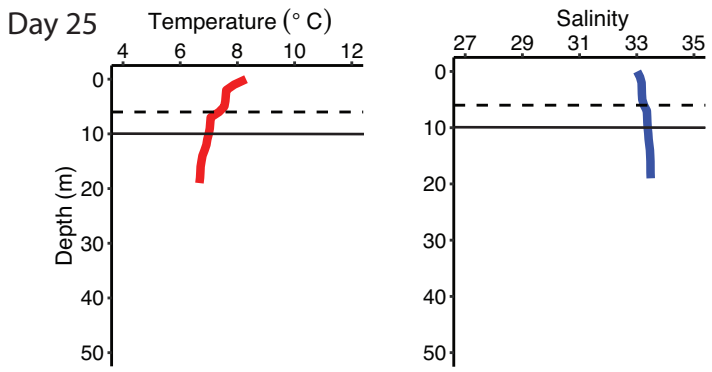


**Supplementary Figure S2 continues.**

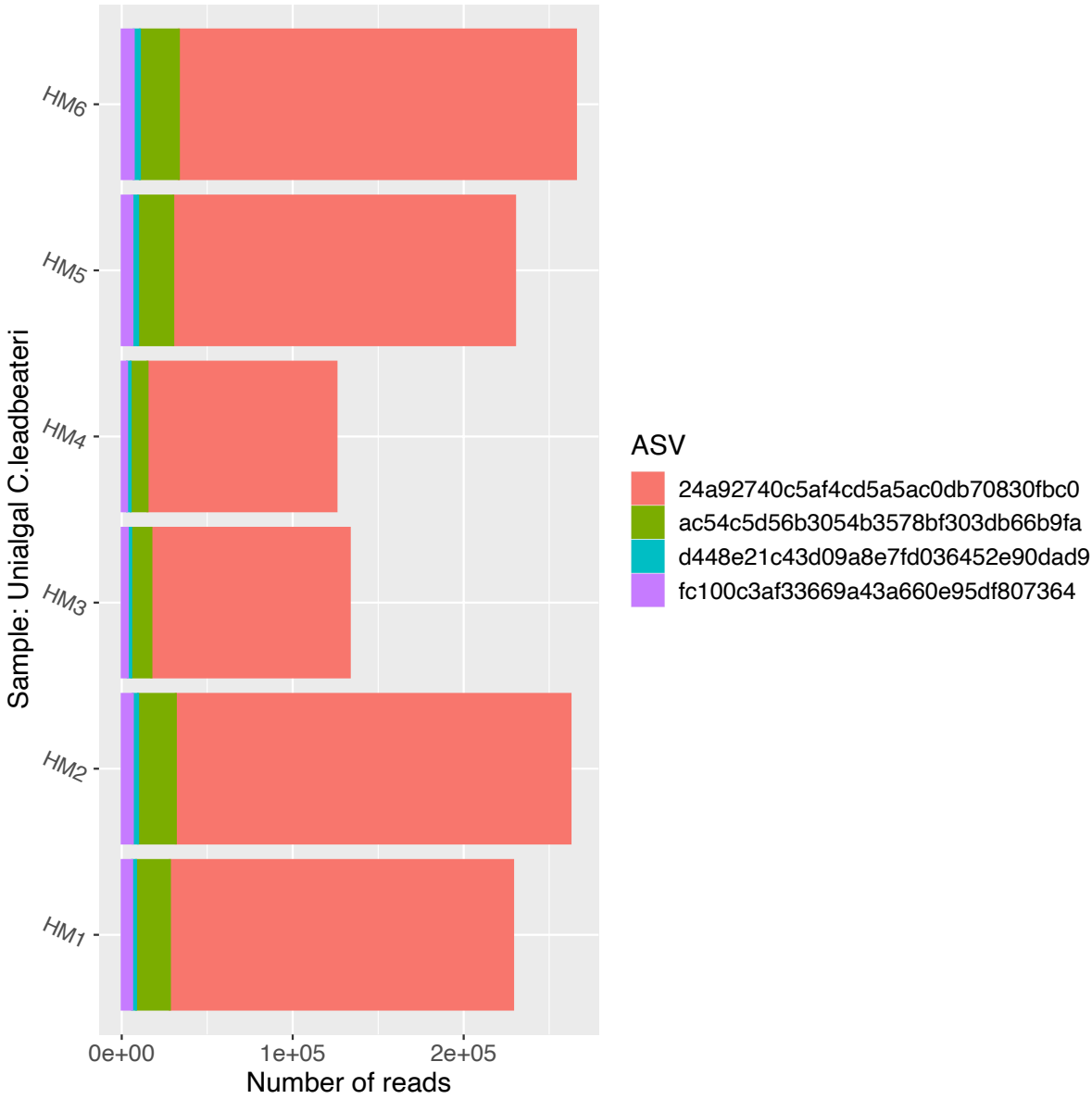


**Supplementary Figure S3.** Number of amplicon sequence reads of each ASV assigned to OLI16029, in unialgal *Chrysochromulina leadbeateri* UiO-035 control culture.

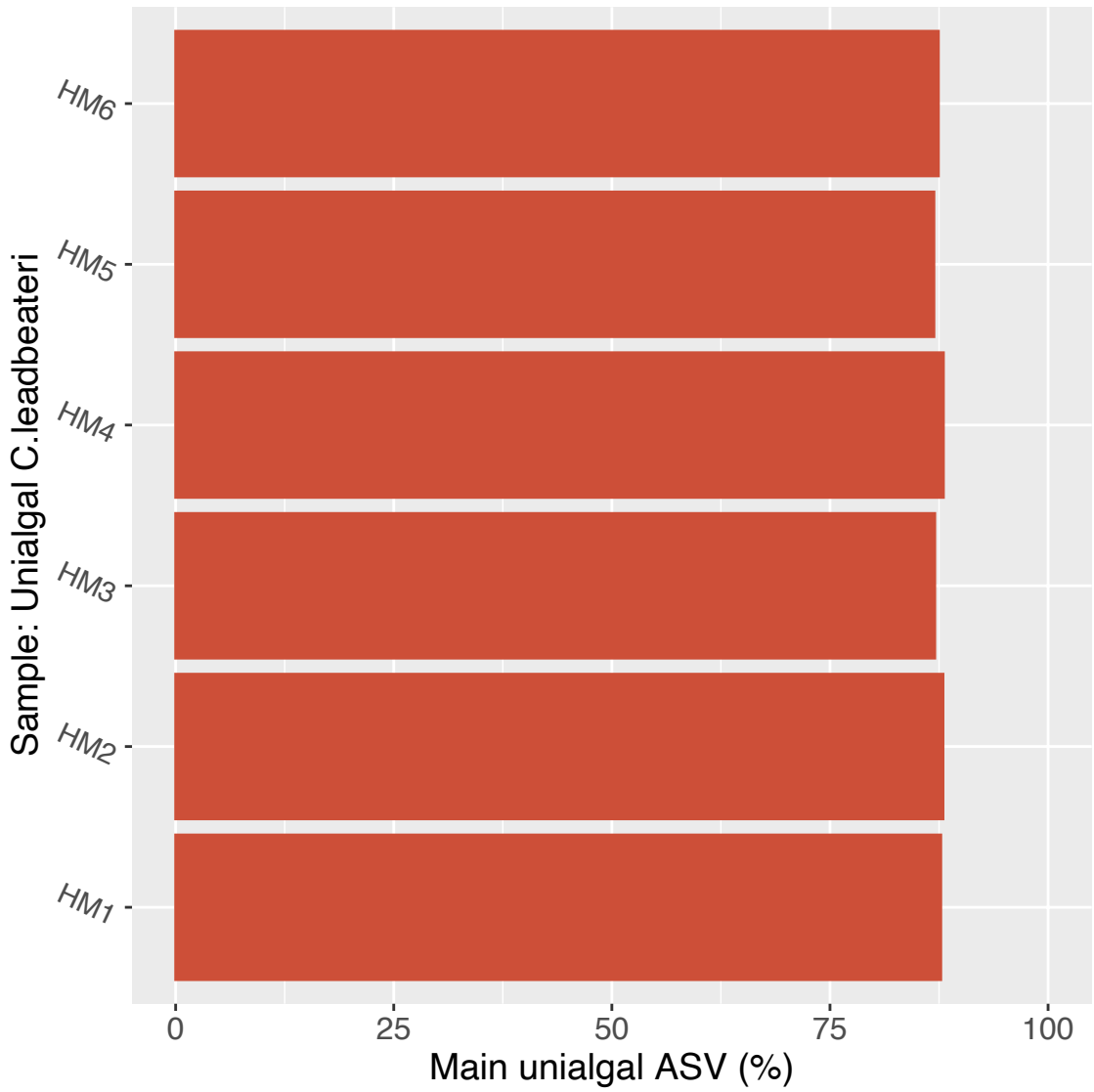


963

964 **Supplementary Figure S4.** Relative abundance of the most abundant ASV

965 (*24a92740c5af4cd5a5ac0db70830fbc0*, referred as a focal ASV) in unialgal

966 *Chrysochromulina leadbeateri* UiO-035 control culture among all the ASVs assigned to

967 OLI16029.

968

969

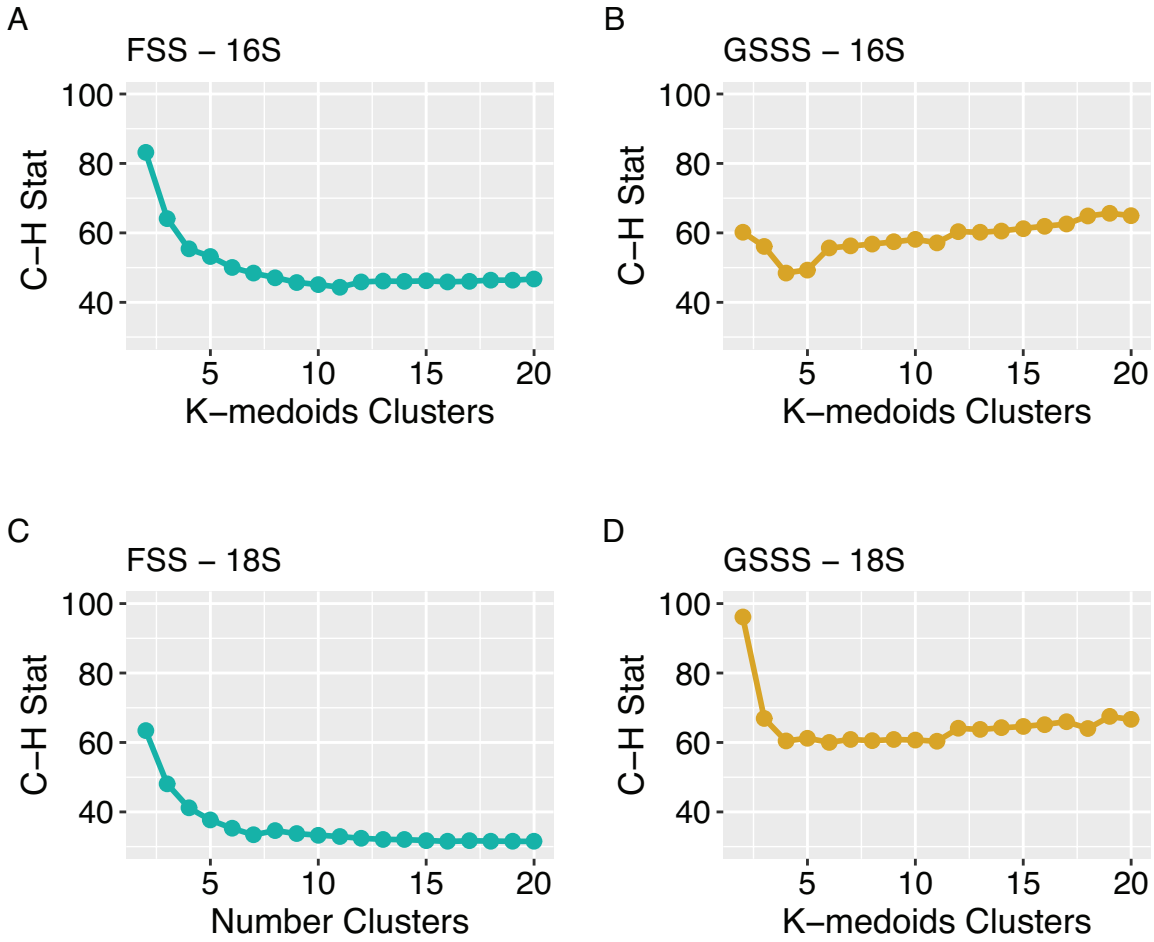


**Supplementary Figure S5.** The Calinski-Harabasz index (y-axis, C-H Stat) was used to determine the number of K-medoids clusters. C-H Stat is a normalized ratio of the inter and intra cluster variance calculated for each sample-specific K-medoids cluster. High C-H Stat value indicates more uniquely portioned clusters. A) Three clusters were chosen to represent 16S ASVs from FSS time series. B) Three clusters were chosen to represent 16S ASVs from the from GSSS time series. C) Four clusters were chosen to represent 18S ASVs from FSS time series. D) Three clusters were chosen to represent 18S ASVs from the from GSSS time series.

987 **Supplementary Table 3.** Results of perMANOVA pariwise comparison between 1) time
988 series sample stations, 2) sample weeks and 3) sample days within each sample station for
989 prokaryotic and microeukaryotic communities, respectively. Unweighted UniFrac was used as
990 a distance metric, and number of permutations was 999.
991

| Groups | R2 | r | p.value | Data type | Station |
|---|---|---|---|---|---|
| FSS vs GSSS | 0.3 | 0.54 | 0.001 | 16S | |
| FSS vs GSSS | 0.46 | 0.68 | 0.001 | 18S | |
| Week_0 vs Week_1 | 0.22 | 0.47 | 0.001 | 16S | FSS |
| Week_0 vs Week_2 | 0.16 | 0.39 | 0.002 | 16S | FSS |
| Week_0 vs Week_3 | 0.21 | 0.45 | 0.001 | 16S | FSS |
| Week_1 vs Week_2 | 0.25 | 0.5 | 0.001 | 16S | FSS |
| Week_1 vs Week_3 | 0.17 | 0.41 | 0.001 | 16S | FSS |
| Week_2 vs Week_3 | 0.13 | 0.36 | 0.001 | 16S | FSS |
| Week_0 vs Week_1 | 0.08 | 0.28 | 0.013 | 16S | GSSS |
| Week_0 vs Week_2 | 0.16 | 0.4 | 0.001 | 16S | GSSS |
| Week_0 vs Week_3 | 0.21 | 0.46 | 0.001 | 16S | GSSS |
| Week_1 vs Week_2 | 0.14 | 0.38 | 0.001 | 16S | GSSS |
| Week_1 vs Week_3 | 0.23 | 0.48 | 0.001 | 16S | GSSS |
| Week_2 vs Week_3 | 0.11 | 0.32 | 0.003 | 16S | GSSS |
| Week_0 vs Week_1 | 0.38 | 0.61 | 0.002 | 18S | FSS |
| Week_0 vs Week_2 | 0.33 | 0.58 | 0.001 | 18S | FSS |
| Week_0 vs Week_3 | 0.34 | 0.58 | 0.001 | 18S | FSS |
| Week_1 vs Week_2 | 0.42 | 0.65 | 0.002 | 18S | FSS |
| Week_1 vs Week_3 | 0.27 | 0.51 | 0.001 | 18S | FSS |
| Week_2 vs Week_3 | 0.24 | 0.49 | 0.001 | 18S | FSS |
| Week_0 vs Week_1 | 0.08 | 0.28 | 0.024 | 18S | GSSS |
| Week_0 vs Week_2 | 0.16 | 0.4 | 0.001 | 18S | GSSS |
| Week_0 vs Week_3 | 0.21 | 0.46 | 0.001 | 18S | GSSS |
| Week_1 vs Week_2 | 0.14 | 0.38 | 0.003 | 18S | GSSS |
| Week_1 vs Week_3 | 0.23 | 0.48 | 0.001 | 18S | GSSS |
| Week_2 vs Week_3 | 0.11 | 0.32 | 0.003 | 18S | GSSS |
| 0 vs 3 | 0.11 | 0.33 | 0.356 | 16S | FSS |
| 0 vs 7 | 0.32 | 0.57 | 0.003 | 16S | FSS |
| 0 vs 15 | 0.24 | 0.49 | 0.01 | 16S | FSS |
| 0 vs 17 | 0.27 | 0.52 | 0.006 | 16S | FSS |
| 0 vs 21 | 0.29 | 0.54 | 0.001 | 16S | FSS |
| 0 vs 24 | 0.36 | 0.6 | 0.007 | 16S | FSS |
| 3 vs 7 | 0.25 | 0.5 | 0.009 | 16S | FSS |
| 3 vs 15 | 0.21 | 0.46 | 0.006 | 16S | FSS |
| 3 vs 17 | 0.24 | 0.49 | 0.007 | 16S | FSS |
| 3 vs 21 | 0.25 | 0.5 | 0.005 | 16S | FSS |
| 3 vs 24 | 0.29 | 0.54 | 0.005 | 16S | FSS |
| 7 vs 15 | 0.36 | 0.6 | 0.004 | 16S | FSS |

| | | | | | |
|---|---|---|---|---|---|
| 7 vs 17 | 0.29 | 0.54 | 0.003 | 16S | FSS |
| 7 vs 21 | 0.29 | 0.54 | 0.006 | 16S | FSS |
| 7 vs 24 | 0.23 | 0.48 | 0.004 | 16S | FSS |
| 15 vs 17 | 0.22 | 0.47 | 0.009 | 16S | FSS |
| 15 vs 21 | 0.22 | 0.46 | 0.004 | 16S | FSS |
| 15 vs 24 | 0.36 | 0.6 | 0.001 | 16S | FSS |
| 17 vs 21 | 0.16 | 0.4 | 0.01 | 16S | FSS |
| 17 vs 24 | 0.27 | 0.52 | 0.003 | 16S | FSS |
| 21 vs 24 | 0.25 | 0.5 | 0.004 | 16S | FSS |
| 1 vs 4 | 0.28 | 0.53 | 0.002 | 16S | GSSS |
| 1 vs 8 | 0.23 | 0.48 | 0.004 | 16S | GSSS |
| 1 vs 11 | 0.31 | 0.56 | 0.006 | 16S | GSSS |
| 1 vs 16 | 0.34 | 0.59 | 0.004 | 16S | GSSS |
| 1 vs 18 | 0.4 | 0.63 | 0.005 | 16S | GSSS |
| 1 vs 22 | 0.29 | 0.54 | 0.002 | 16S | GSSS |
| 1 vs 25 | 0.36 | 0.6 | 0.002 | 16S | GSSS |
| 4 vs 8 | 0.18 | 0.43 | 0.002 | 16S | GSSS |
| 4 vs 11 | 0.14 | 0.38 | 0.009 | 16S | GSSS |
| 4 vs 16 | 0.17 | 0.42 | 0.002 | 16S | GSSS |
| 4 vs 18 | 0.37 | 0.61 | 0.003 | 16S | GSSS |
| 4 vs 22 | 0.31 | 0.56 | 0.004 | 16S | GSSS |
| 4 vs 25 | 0.37 | 0.61 | 0.004 | 16S | GSSS |
| 8 vs 11 | 0.21 | 0.46 | 0.001 | 16S | GSSS |
| 8 vs 16 | 0.2 | 0.44 | 0.002 | 16S | GSSS |
| 8 vs 18 | 0.33 | 0.58 | 0.002 | 16S | GSSS |
| 8 vs 22 | 0.27 | 0.52 | 0.004 | 16S | GSSS |
| 8 vs 25 | 0.32 | 0.56 | 0.004 | 16S | GSSS |
| 11 vs 16 | 0.19 | 0.43 | 0.007 | 16S | GSSS |
| 11 vs 18 | 0.41 | 0.64 | 0.002 | 16S | GSSS |
| 11 vs 22 | 0.34 | 0.58 | 0.002 | 16S | GSSS |
| 11 vs 25 | 0.38 | 0.62 | 0.002 | 16S | GSSS |
| 16 vs 18 | 0.32 | 0.56 | 0.004 | 16S | GSSS |
| 16 vs 22 | 0.27 | 0.52 | 0.001 | 16S | GSSS |
| 16 vs 25 | 0.32 | 0.56 | 0.003 | 16S | GSSS |
| 18 vs 22 | 0.15 | 0.38 | 0.005 | 16S | GSSS |
| 18 vs 25 | 0.24 | 0.49 | 0.003 | 16S | GSSS |
| 22 vs 25 | 0.18 | 0.42 | 0.004 | 16S | GSSS |
| 0 vs 3 | 0.19 | 0.43 | 0.017 | 18S | FSS |
| 0 vs 7 | 0.48 | 0.69 | 0.002 | 18S | FSS |
| 0 vs 15 | 0.5 | 0.71 | 0.008 | 18S | FSS |
| 0 vs 17 | 0.47 | 0.69 | 0.009 | 18S | FSS |
| 0 vs 21 | 0.44 | 0.67 | 0.004 | 18S | FSS |
| 0 vs 24 | 0.56 | 0.75 | 0.001 | 18S | FSS |

| | | | | | |
|---|---|---|---|---|---|
| 3 vs 7 | 0.42 | 0.65 | 0.002 | 18S | FSS |
| 3 vs 15 | 0.44 | 0.66 | 0.003 | 18S | FSS |
| 3 vs 17 | 0.4 | 0.63 | 0.002 | 18S | FSS |
| 3 vs 21 | 0.37 | 0.61 | 0.001 | 18S | FSS |
| 3 vs 24 | 0.49 | 0.7 | 0.004 | 18S | FSS |
| 7 vs 15 | 0.54 | 0.74 | 0.006 | 18S | FSS |
| 7 vs 17 | 0.44 | 0.66 | 0.002 | 18S | FSS |
| 7 vs 21 | 0.41 | 0.64 | 0.005 | 18S | FSS |
| 7 vs 24 | 0.37 | 0.61 | 0.002 | 18S | FSS |
| 15 vs 17 | 0.31 | 0.56 | 0.007 | 18S | FSS |
| 15 vs 21 | 0.35 | 0.59 | 0.002 | 18S | FSS |
| 15 vs 24 | 0.54 | 0.74 | 0.002 | 18S | FSS |
| 17 vs 21 | 0.23 | 0.48 | 0.001 | 18S | FSS |
| 17 vs 24 | 0.44 | 0.66 | 0.004 | 18S | FSS |
| 21 vs 24 | 0.31 | 0.55 | 0.004 | 18S | FSS |
| 1 vs 4 | 0.28 | 0.53 | 0.002 | 18S | GSSS |
| 1 vs 8 | 0.23 | 0.48 | 0.001 | 18S | GSSS |
| 1 vs 11 | 0.31 | 0.56 | 0.004 | 18S | GSSS |
| 1 vs 16 | 0.34 | 0.59 | 0.003 | 18S | GSSS |
| 1 vs 18 | 0.4 | 0.63 | 0.002 | 18S | GSSS |
| 1 vs 22 | 0.29 | 0.54 | 0.003 | 18S | GSSS |
| 1 vs 25 | 0.36 | 0.6 | 0.007 | 18S | GSSS |
| 4 vs 8 | 0.18 | 0.43 | 0.002 | 18S | GSSS |
| 4 vs 11 | 0.14 | 0.38 | 0.008 | 18S | GSSS |
| 4 vs 16 | 0.17 | 0.42 | 0.009 | 18S | GSSS |
| 4 vs 18 | 0.37 | 0.61 | 0.001 | 18S | GSSS |
| 4 vs 22 | 0.31 | 0.56 | 0.003 | 18S | GSSS |
| 4 vs 25 | 0.37 | 0.61 | 0.005 | 18S | GSSS |
| 8 vs 11 | 0.21 | 0.46 | 0.002 | 18S | GSSS |
| 8 vs 16 | 0.2 | 0.44 | 0.005 | 18S | GSSS |
| 8 vs 18 | 0.33 | 0.58 | 0.003 | 18S | GSSS |
| 8 vs 22 | 0.27 | 0.52 | 0.005 | 18S | GSSS |
| 8 vs 25 | 0.32 | 0.56 | 0.004 | 18S | GSSS |
| 11 vs 16 | 0.19 | 0.43 | 0.012 | 18S | GSSS |
| 11 vs 18 | 0.41 | 0.64 | 0.001 | 18S | GSSS |
| 11 vs 22 | 0.34 | 0.58 | 0.004 | 18S | GSSS |
| 11 vs 25 | 0.38 | 0.62 | 0.002 | 18S | GSSS |
| 16 vs 18 | 0.32 | 0.56 | 0.003 | 18S | GSSS |
| 16 vs 22 | 0.27 | 0.52 | 0.006 | 18S | GSSS |
| 16 vs 25 | 0.32 | 0.56 | 0.002 | 18S | GSSS |
| 18 vs 22 | 0.15 | 0.38 | 0.004 | 18S | GSSS |
| 18 vs 25 | 0.24 | 0.49 | 0.006 | 18S | GSSS |
| 22 vs 25 | 0.18 | 0.42 | 0.004 | 18S | GSSS |

992 **Supplementary Table S4.** Summary of physical environmental measurements and analyzed
993 inorganic nutrients as well as the relative abundance of Focal taxon, OLI16029. Mean values
994 and (min, max) are shown.
995

| | Station | |
|---|---|---|
| | FSS | GSSS |
| Temperature (°C)[a] | 6.6<br>(5.4, 7.4) | 6.2<br>(5.3, 7.0) |
| Salinity[a] | 33.1<br>(32.5, 33.4) | 33.4<br>(33.2, 33.6) |
| MLD (m) | 3<br>(3.3) | 5<br>(3, 7) |
| $Si(OH)_4$ (μmol $L^{-1}$) | 1.24<br>(0.69, 1.87) | 1.56<br>(0.09, 3.00) |
| $NO_2^-$ + $NO_3^-$ (μmol $L^{-1}$) | 0.18<br>(0.07, 0.41) | 0.43<br>(0.09, 1.20) |
| $PO_4^{3-}$ (μmol $L^{-1}$) | 0.06<br>(< 0.04, 0.12) | 0.07<br>(< 0.04, 0.39) |
| Focal taxon (%)[b] | 0.7<br>(0.4, 1.3) | 3.4<br>(0.02, 17.7) |

996 [a] Values at the depth of 10 m
997 [b] Relative abundance of ASVs assigned to OLI16029
998

999

1000

1001

1002

1003

1004

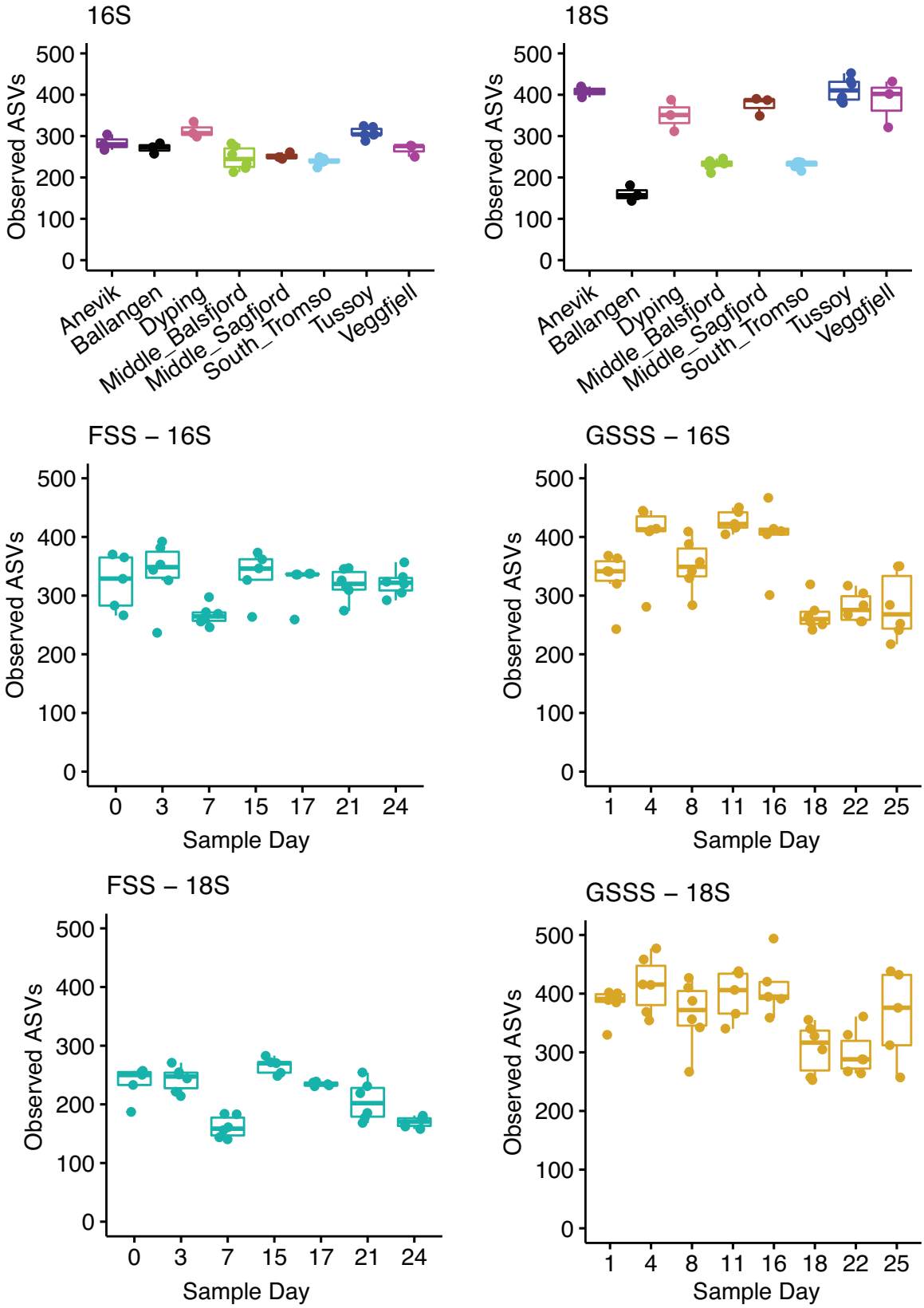


**Supplementary Figure S6.** Alpha diversity as observed number of ASVs per sample set: single-time-point stations and time series stations.